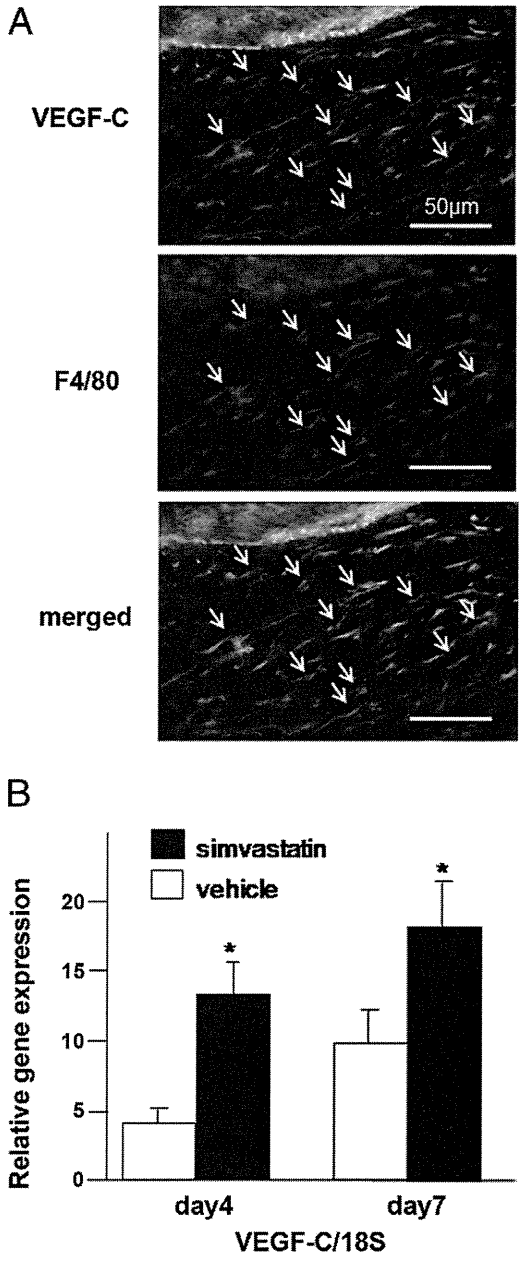

Figure 7. VEGF-C expression in granulation tissue. **A:** Representative photomicrographs of the immunostained wound edge treated with simvastatin at 7 days after wound creation. Green and red fluorescence indicates VEGF-C expression and F4/80-positive macrophages, respectively. Original magnification, ×400. **Arrows** indicate double-positive cells. Scale bar = 50 μm. **B:** Quantitative RT-PCR of VEGF-C in wound granulation tissue. Gene expression levels were normalized based on the level of an internal reference gene, 18S. $^*P < 0.05$ versus vehicle ($n = 5$).

new therapeutic strategy for treatment of local ischemic conditions, such as those in patients with diabetic ulcers.

Lymphangiogenesis is a major factor in diabetic refractory wound healing.[4,5] Therefore, we focused on the effects of simvastatin on wound lymphangiogenesis. Recent studies have suggested that several biological functions of LECs are partially regulated by the AKT/PI3K/mTOR pathway.[25,26] Consistent with these observations, capillary morphogenesis of LECs was significantly stimulated by simvastatin as an effect on vascular endothelial cells that was, at least in part, regulated by the AKT/PI3K/mTOR pathway. Our results suggest that the mechanisms underlying the lymphangiogenic effects of simvastatin in LECs might be similar to those for angiogenic effects. These mechanisms include antiapoptosis and promotion of capillary morphogenesis because LECs develop from a vascular network in an embryonic stage,[27] and these cells have a similar lineage. However, contrary to our expectation, simvastatin did not promote proliferation of LECs *in vitro*. During the wound healing process, new lymphatics are formed in newly generated granulation tissue, indicating that proliferation of preexisting lymphatic vessels is needed.

Because simvastatin did not promote the proliferation of LECs, we evaluated other possible sources of lymphangiogenic factors. Several reports suggest that infiltrating macrophages contribute to lymphangiogenesis as the major producer of VEGF-C in cutaneous wound healing,[4,5] and therefore we evaluated the effects of simvastatin on macrophages. Macrophages carry VEGF receptor 3, in addition to producing VEGF-C, and thus act as both autocrine and paracrine factors. We have previously reported that healing impairment in diabetes involves reduced lymphangiogenesis and suppressed macrophage function, such as recruitment to inflammatory sites and secretion of growth factors.[5] In this study, the number of infiltrating macrophages in granulation tissue was significantly increased by topical application of simvastatin, and most of these macrophages produced VEGF-C. These observations suggest that simvastatin recovers lymphangiogenic function that is impaired in macrophages under diabetic conditions.

Increased apoptosis is a major concern in wound healing in a diabetic state.[3,28–31] Hyperglycemia induces proinflammatory cytokines, such as TNF-α, and oxidative stress, which result in increased apoptosis in diabetes. Our study found that most infiltrating macrophages in diabetic wounds had an M1 proinflammatory phenotype producing abundant TNF-α. Simvastatin decreased H_2O_2-induced apoptosis in LECs *in vitro* and increased M2 anti-inflammatory phenotype macrophages in granulation tissue *in vivo*. We suggest that this anti-apoptotic effect of simvastatin also plays an important role, in addition to promotion of angiogenesis and lymphangiogenesis.

Increased infiltration of macrophages induced by simvastatin may have further benefits because the histologic scores of diabetic wounds were significantly improved by topical application of simvastatin. The histologic score reflects the degree of maturation of granulation tissue, including inflammation, collagen deposition, and reepithelialization, in addition to neovascularization. Macrophages play a central role in all stages of wound healing and orchestrate the wound healing process[32] by exerting proinflammatory functions and facilitating wound healing during the early stage and stimulating proliferation of fibroblasts, keratinocytes, and endothelial cells in the proliferative stage. Because the main focus of this study was lymphangiogenesis, we did not investigate the effects of simvastatin on reepithelialization or formation of extracellular matrix. This will require further experiments in a future study.

In conclusion, regulation of apoptosis and capillary differentiation are essential for development of functional lymphatics during wound healing. The findings of the present study suggest that topical simvastatin can stimulate lymp-

hangiogenesis directly and indirectly via stimulation of macrophages. Vascular remodeling induced by simvastatin might have therapeutic potential in patients with microvascular dysfunction, such as that in diabetic foot ulcer, a major cause of morbidity in the growing population of patients with diabetes. A future investigation is warranted to determine the potential clinical utility of this approach.

References

1. Jeffcoate WJ, Harding KG: Diabetic foot ulcers. Lancet 2003, 361: 1545–1551
2. Lerman OZ, Galiano RD, Armour M, Levine JP, Gurtner GC: Cellular dysfunction in the diabetic fibroblast: impairment in migration, vascular endothelial growth factor production, and response to hypoxia. Am J Pathol 2003, 162:303–312
3. Fadini GP, Albiero M, Menegazzo L, Boscaro E, Pagnin E, Iori E, Cosma C, Lapolla A, Pengo V, Stendardo M, Agostini C, Pelicci PG, Giorgio M, Avogaro A: The redox enzyme p66Shc contributes to diabetes and ischemia-induced delay in cutaneous wound healing. Diabetes 2010, 59:2306–2314
4. Saaristo A, Tammela T, Farkkila A, Karkkainen M, Suominen E, Yla-Herttuala S, Alitalo K: Vascular endothelial growth factor-C accelerates diabetic wound healing. Am J Pathol 2006, 169:1080–1087
5. Maruyama K, Asai J, Ii M, Thorne T, Losordo DW, D'Amore PA: Decreased macrophage number and activation lead to reduced lymphatic vessel formation and contribute to impaired diabetic wound healing. Am J Pathol 2007, 170:1178–1191
6. Oliver G, Detmar M: The rediscovery of the lymphatic system: old and new insights into the development and biological function of the lymphatic vasculature. Genes Dev 2002, 16:773–783
7. Witte MH, Bernas MJ, Martin CP, Witte CL: Lymphangiogenesis and lymphangiodysplasia: from molecular to clinical lymphology. Microsc Res Tech 2001, 55:122–145
8. Ji RC: Characteristics of lymphatic endothelial cells in physiological and pathological conditions. Histol Histopathol 2005, 20:155–175
9. Werner N, Nickenig G, Laufs U: Pleiotropic effects of HMG-CoA reductase inhibitors. Basic Res Cardiol 2002, 97:105–116
10. Landmesser U, Engberding N, Bahlmann FH, Schaefer A, Wiencke A, Heineke A, Spiekermann S, Hilfiker-Kleiner D, Templin C, Kotlarz D, Mueller M, Fuchs M, Hornig B, Haller H, Drexler H: Statin-induced improvement of endothelial progenitor cell mobilization, myocardial neovascularization, left ventricular function, and survival after experimental myocardial infarction requires endothelial nitric oxide synthase. Circulation 2004, 110:1933–1939
11. Kureishi Y, Luo Z, Shiojima I, Bialik A, Fulton D, Lefer DJ, Sessa WC, Walsh K: The HMG-CoA reductase inhibitor simvastatin activates the protein kinase Akt and promotes angiogenesis in normocholesterolemic animals. Nat Med 2000, 6:1004–1010
12. Bitto A, Minutoli L, Altavilla D, Polito F, Fiumara T, Marini H, Galeano M, Calo M, Lo Cascio P, Bonaiuto M, Migliorato A, Caputi AP, Squadrito F: Simvastatin enhances VEGF production and ameliorates impaired wound healing in experimental diabetes. Pharmacol Res 2008, 57:159–169
13. Emanueli C, Monopoli A, Kraenkel N, Meloni M, Gadau S, Campesi I, Ongini E, Madeddu P: Nitropravastatin stimulates reparative neovascularisation and improves recovery from limb ischaemia in type-1 diabetic mice. Br J Pharmacol 2007, 150:873–882
14. Otuki MF, Pietrovski EF, Cabrini DA: Topical simvastatin: preclinical evidence for a treatment of skin inflammatory conditions. J Dermatol Sci 2006, 44:45–47
15. Greenhalgh DG, Sprugel KH, Murray MJ, Ross R: PDGF and FGF stimulate wound healing in the genetically diabetic mouse. Am J Pathol 1990, 136:1235–1246
16. Asai J, Takenaka H, Katoh N, Kishimoto S: Dibutyryl cAMP influences endothelial progenitor cell recruitment during wound neovascularization. J Invest Dermatol 2006, 126:1159–1167
17. Asai J, Takenaka H, Kusano KF, Ii M, Luedemann C, Curry C, Eaton E, Iwakura A, Tsutsumi Y, Hamada H, Kishimoto S, Thorne T, Kishore R, Losordo DW: Topical sonic hedgehog gene therapy accelerates wound healing in diabetes by enhancing endothelial progenitor cell-mediated microvascular remodeling. Circulation 2006, 113:2413–2424
18. Abràmoff MD, Magalhães PJ, Ram S: J: image processing with ImageJ. Biophotonics Int 2004, 11:36–42
19. Jacobi J, Jang JJ, Sundram U, Dayoub H, Fajardo LF, Cooke JP: Nicotine accelerates angiogenesis and wound healing in genetically diabetic mice. Am J Pathol 2002, 161:97–104
20. Hirakawa S, Hong YK, Harvey N, Schacht V, Matsuda K, Libermann T, Detmar M: Identification of vascular lineage-specific genes by transcriptional profiling of isolated blood vascular and lymphatic endothelial cells. Am J Pathol 2003, 162:575–586
21. Maruyama K, Ii M, Cursiefen C, Jackson DG, Keino H, Tomita M, Van Rooijen N, Takenaka H, D'Amore PA, Stein-Streilein J, Losordo DW, Streilein JW: Inflammation-induced lymphangiogenesis in the cornea arises from CD11b-positive macrophages. J Clin Invest 2005, 115:2363–2372
22. Nakao T, Shiota M, Tatemoto Y, Izumi Y, Iwao H: Pravastatin induces rat aortic endothelial cell proliferation and migration via activation of PI3K/Akt/mTOR/p70 S6 kinase signaling. J Pharmacol Sci 2007, 105:334–341
23. Cantoni S, Cavallini C, Bianchi F, Bonavita F, Vaccari V, Olivi E, Frascari I, Tassinari R, Valente S, Lionetti V, Ventura C: Rosuvastatin elicits KDR-dependent vasculogenic response of human placental stem cells through PI3K/AKT pathway. Pharmacol Res 2012, 65:275–284
24. Zhao TT, Trinh D, Addison CL, Dimitroulakos J: Lovastatin inhibits VEGFR and AKT activation: synergistic cytotoxicity in combination with VEGFR inhibitors. PLoS One 2010, 5:e12563
25. Luo Y, Liu L, Rogers D, Su W, Odaka Y, Zhou H, Chen W, Shen T, Alexander JS, Huang S: Rapamycin inhibits lymphatic endothelial cell tube formation by downregulating vascular endothelial growth factor receptor 3 protein expression. Neoplasia 2012, 14:228–237
26. Dellinger MT, Brekken RA: Phosphorylation of Akt and ERK1/2 is required for VEGF-A/VEGFR2-induced proliferation and migration of lymphatic endothelium. PLoS One 2011, 6:e28947
27. Oliver G: Lymphatic vasculature development. Nat Rev Immunol 2004, 4:35–45
28. Hamed S, Ullmann Y, Egozi D, Daod E, Hellou E, Ashkar M, Gilhar A, Teot L: Fibronectin potentiates topical erythropoietin-induced wound repair in diabetic mice. J Invest Dermatol 2011, 131:1365–1374
29. Badr G: Supplementation with undenatured whey protein during diabetes mellitus improves the healing and closure of diabetic wounds through the rescue of functional long-lived wound macrophages. Cell Physiol Biochem 2012, 29:571–582
30. Ahmad J, Zubair M, Malik A, Siddiqui MA, Wangnoo SK: Cathepsin-D, Adiponectin, TNF-alpha, IL-6 and hsCRP plasma levels in subjects with diabetic foot and possible correlation with clinical variables: a multicentric study. Foot (Edinb) 2012, 22:194–199
31. Dave GS, Kalia K: Hyperglycemia induced oxidative stress in type-1 and type-2 diabetic patients with and without nephropathy. Cell Mol Biol (Noisy-le-grand) 2007, 53:68–78
32. Mahdavian Delavary B, van der Veer WM, van Egmond M, Niessen FB, Beelen RH: Macrophages in skin injury and repair. Immunobiology 2011, 216:753–762

Naoki Sasaki[1]
Mika Shinjo[1]
Satoshi Hirakawa[2]
Masahiro Nishinaka[3]
Yo Tanaka[3]
Kazuma Mawatari[3,4]
Takehiko Kitamori[3,4]
Kae Sato[1,4]

[1]Department of Chemical and Biological Sciences, Faculty of Science, Japan Women's University, Mejirodai, Bunkyo-ku, Tokyo, Japan
[2]Department of Dermatology, Hamamatsu University School of Medicine, Handayama, Higashi-ku, Hamamatsu, Shizuoka, Japan
[3]Department of Applied Chemistry, Graduate School of Engineering, The University of Tokyo, Hongo, Bunkyo-ku, Tokyo, Japan
[4]Core Research for Evolutional Science and Technology (CREST), Japan Science and Technology Agency, Kawaguchi, Saitama, Japan

Received December 14, 2011
Revised March 8, 2012
Accepted March 13, 2012

Research Article

A palmtop-sized microfluidic cell culture system driven by a miniaturized infusion pump

A palmtop-sized microfluidic cell culture system is presented. The system consists of a microfluidic device and a miniaturized infusion pump that possesses a reservoir of culture medium, an electrical control circuit, and an internal battery. The footprint of the system was downsized to 87 × 57 mm, which is, to the best of our knowledge, the smallest integrated cell culture system. Immortalized human microvascular endothelial cells (HMEC-1) and human umbilical vein endothelial cells (HUVEC) were cultured in the system. HMEC-1 in the system proliferated at the same speed as cells in a microchannel perfused by a syringe pump and cells in a culture flask. HUVEC in the system oriented along the direction of the fluid flow. Claudin-5, a tight junction protein, was localized along the peripheries of the HUVEC. We expect that the present system is applicable to various cell types as a stand-alone and easy-to-use system for microfluidic bioanalysis.

Keywords:
Endothelial cells / Orientation / Perfusion culture / Proliferation / Tight junctions
DOI 10.1002/elps.201100691

1 Introduction

Microfluidic devices are among the attractive platforms for cell separation, cell culture, and cell-based assays [1, 2]. For example, microfluidic devices have been utilized for hydrodynamic [3] and acoustophoretic [4] separation of cells. On the other hand, cell cultures and subsequent assay of cells in a microchannel have also been studied. The size of a microchannel is smaller than that of a cell culture flask, and the number of cells and amount of reagents utilized can therefore be reduced. Moreover, multiple microchannels and microchambers can be easily fabricated on a single device [5], and various applications such as fast and high throughput analyses by parallelization are expected.

Various types of cells have been cultured on microfluidic devices, such as endothelial cells located at the inner surface of blood vessels [6]. The size of the microchannel is comparable to that of blood vessels, and shear stress due to fluid flow is applied to the endothelial cells cultured in the microchannel. In fact, a number of microfluidic devices for vascular research have been reported. The devices have been applied to various experiments, including cell culture [7–10], cell adhesion assay [11, 12], shear stress response analysis [13–21], permeability measurement [22, 23], and transendothelial electric resistance (TEER) measurement [24, 25]. Another example of a cell cultured on microfluidic devices is the osteoblastic cell [26, 27]. The cell is responsive to shear stress due to fluid flow, which is easily controlled by channel dimensions and flow velocity. We have also developed cell-based microfluidic devices [28], and have reported a leukocyte adhesion assay on endothelial cells [29], recovery of cultured endothelial cells from a separable microfluidic device [30], and the automated long-term monitoring of alkaline phosphatase activity of osteoblastic cells [31].

Pumping of fluids into a microchannel is important for cell-based microfluidic devices. For example, it is necessary to pump medium for a perfusion culture and to introduce reagents for assays. Various pumping methods for cell-based microfluidic devices have been reported. Pumping by hydrostatic pressure is simple and has been utilized by various

Correspondence: Professor Kae Sato, Department of Chemical and Biological Sciences, Faculty of Science, Japan Women's University, 2-8-1 Mejirodai, Bunkyo-ku, Tokyo 112-8681, Japan
E-mail: satouk@fc.jwu.ac.jp
Fax: +81-3-5981-3661

Abbreviations: HMEC-1, immortalized human microvascular endothelial cells; **HUVEC**, human umbilical vein endothelial cells; **TEER**, transendothelial electric resistance

Colour Online: See the article online to view Fig. 5 in colour.

studies [8,11,13]. However, the pumping can induce only continuous flow. In contrast, a computer-controlled pump can induce various types of flow, including continuous flow and pulsatile flow, at various flow rates. Both a syringe pump and a peristaltic pump have been utilized for cell-based microfluidic devices. However, the commercially available pumps are generally larger than microfluidic devices, an aspect that limits downsizing of the whole system. An integrated culture system driven by a peristaltic pump has been reported [32], but it requires a large medium reservoir and a large motor controller compared to the device. Microfabricated peristaltic pumps have been utilized to analyze secreted molecules from cells [33] and to culture cells in microchambers in an automated manner [34]. However, these systems require additional valves and tubes to control the pumps, and the structure of the microfluidic devices becomes complex. A palm-sized cell culture system driven by Braille pins has been reported [35], but it requires external power supply for long-term culture (>2 h).

In this paper, we present a palmtop-sized, stand-alone cell culture system that consists of a microfluidic device and a miniaturized infusion pump. All the required components are integrated into the system, and there is therefore no need for tubes or electrical connections from outside the system. As a result, the footprint of the system can be downsized to 87 × 57 mm. We apply the system to culture both immortalized and normal endothelial cells in a microchannel. Then, we evaluate the culture in terms of proliferation rate, cell orientation under fluid flow, and expression of tight junction proteins. Control experiments are conducted with a microfluidic device and a syringe pump as examples of conventional microfluidic cell culture systems.

2 Materials and methods

2.1 Cells and culture procedures

Immortalized human microvascular endothelial cells (HMEC-1) [36] and human umbilical vein endothelial cells (HUVEC; Lonza, Basel, Switzerland) were selected as representatives of endothelial cell lines and normal human endothelial cells, respectively. HMEC-1 was cultured in a 25-cm^2 cell culture flask (353014, Becton, Dickinson and Company, Franklin Lakes, NJ, USA). The cells were grown in MCDB 131 (Invitrogen, Carlsbad, CA, USA) supplemented with 30% FBS (Invitrogen), 1×GlutaMAX™-I Supplement (Invitrogen), 13 μg mL^{-1} Hydrocortisone (Sigma-Aldrich, St. Louis, MO, USA), and 10 ng mL^{-1} epidermal growth factor (Sigma-Aldrich). HUVEC was cultured in a 25 cm^2 cell culture flask (3289, Corning, NY, USA). The cells were grown in EBM™-2 (Lonza) supplemented with EGM™-2 BulletKit (Lonza). All reported experiments utilized cells between passages 3 and 8.

Once cells reached confluence, the medium in a cell culture flask was aspirated. The cells were rinsed with 5 mL of PBS (TAKARA BIO, Shiga, Japan) and then treated with 500 μL of TrypLE™ Express (Invitrogen). After the cells were detached from the surface of the flask, 1 mL of fresh medium was added, and the obtained cell suspension was added to 4 mL of fresh medium in a 15-mL conical tube. The tube was centrifuged at 1200 rpm for 3 min and the supernatant was aspirated. Finally, the cells were resuspended in the medium at the required concentration.

2.2 Microfabrication

Microfluidic devices were fabricated using standard microfabrication techniques [37]. A negative master for the molding of PDMS was fabricated on a glass slide (S1226, Matsunami Glass, Osaka, Japan) with photoresist (SU-8 50, MicroChem, Newton, MA, USA). The master contained four I-shaped convex patterns, which gave recessed microchannel patterns (300 μm width, 67 μm depth, 20 mm length) to the PDMS part (2 mm thickness) after the molding. The surface of the master was passivated by coating with a fluoropolymer (INT-332VE, Noda Screen, Aichi, Japan). A prepolymer of PDMS (SILPOT 184, Dow Corning, Midland, MI, USA) was poured onto the master with a frame for holding the prepolymer. The prepolymer was cured in an oven at 65°C for 60 min, and the cured PDMS was peeled off from the master, bonded to a virgin glass slide, and cured again at 100°C for 60 min. Through -holes for tubes were punched at the end of the microchannel patterns on the PDMS part using a metal pipe. The PDMS part was then cut into four parts, each of which had the microchannel. Silicone tubes (0.5 mm id, 1.0 mm od, AS ONE, Osaka, Japan) or PTFE tubes (0.46 mm id, 0.92 mm od, NICHIAS, Tokyo, Japan) were glued to the through-holes with the prepolymer at 65°C for 60 min. The PDMS part with the tubes was sterilized in an autoclave at 121°C for 20 min, bonded to the bottom part of a 35-mm cell culture dish (Asahi glass, Tokyo, Japan), and kept in a clean bench until cell culture experiments.

2.3 Microfluidic cell culture systems

Figure 1A and B show microfluidic cell culture systems driven by a syringe pump (model 210, KD Scientific, Holliston, MA, USA). HMEC-1 was cultured in the system shown in Fig. 1A. One of the silicone tubes was connected to a 1-mL syringe (Terumo, Tokyo, Japan) via a metal pipe (0.33 mm id, 0.63 mm od, Nonaka Rikaki, Tokyo, Japan), a perfluoroalkoxy capillary (0.1 mm id, 0.3 mm od, Iwase, Kanagawa, Japan), and a needle (0.33 mm id, 0.63 mm od, Nonaka Rikaki). The other tube was connected to a capillary via a pipe. HUVEC was cultured in the system shown in Fig. 1B. One of the PTFE tubes was connected to a syringe via a bubble trap, a capillary, and a needle. The bubble trap was fabricated in accordance with details provided in the literature [38]. Two TYGON™ tubes (0.79 mm id, 2.38 mm od, Saint-Gobain K.K., Tokyo, Japan) and another TYGON tube (2 mm id, 4 mm od, Saint-Gobain K.K.) were used to compose the trap.

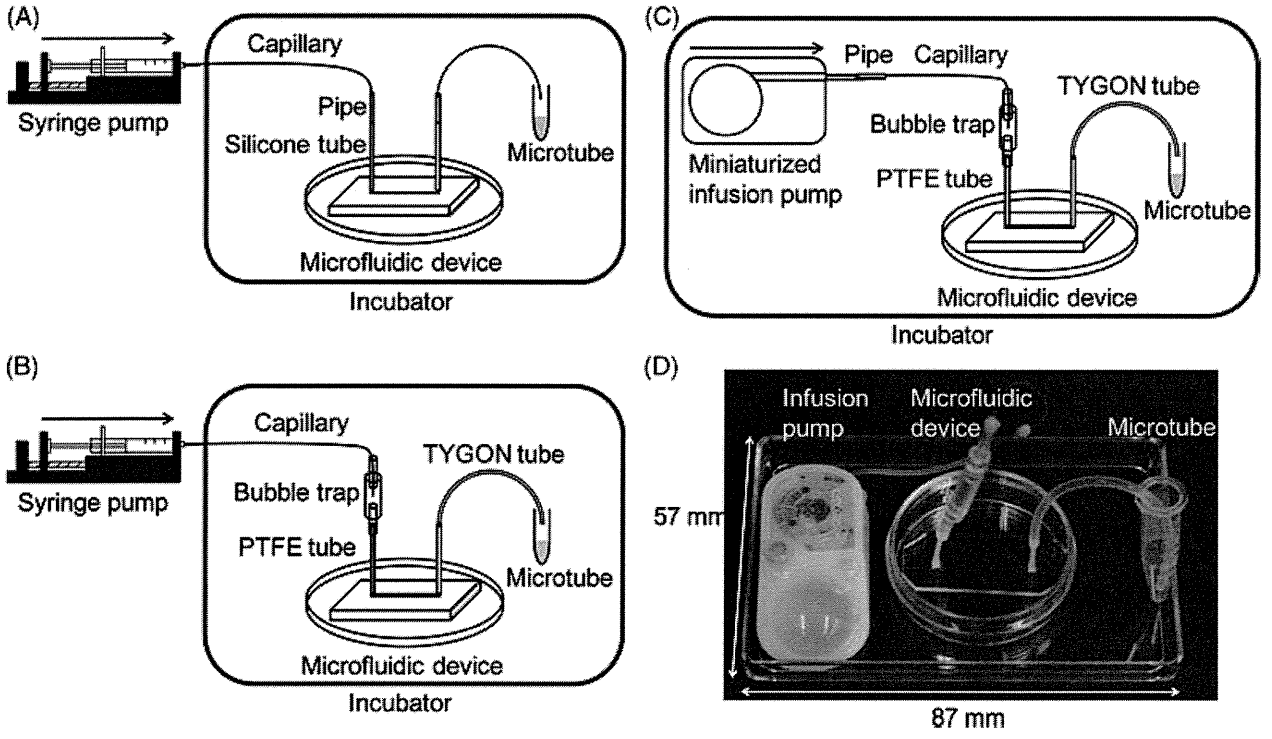

Figure 1. Microfluidic cell culture systems. (A–C) Schematic illustrations of microfluidic cell culture system. (A) A system with a syringe pump. (B) A system with a syringe pump and a bubble trap. (C) A palmtop-sized culture system with a miniaturized infusion pump and a bubble trap. (D) Photograph of the palmtop-sized microfluidic cell culture system.

The other PTFE tube on the microfluidic device was also connected to a TYGON tube. In the palmtop-sized microfluidic cell culture system shown in Fig. 1C, a miniaturized infusion pump (SMP101-L, Primetech, Tokyo, Japan) was used instead of the syringe pump shown in Fig. 1B. The components of the systems were glued with epoxy adhesive as required.

2.4 Cell culture in a microchannel

All the tubes, pipes, and capillaries used in this study were sterilized in an autoclave at 121°C for 20 min. Medium for cell culture was incubated in an incubator for 30 min prior to experiments to equilibrate the concentration of CO_2 in the medium with that in the incubator. Microfluidic devices were degassed in a vacuum desiccator (PC-150K, Sanplatec, Osaka, Japan) connected to a vacuum pump (DAP-6D, Ulvac, Kanagawa, Japan) at 10 kPa for 30 min to prevent air bubbles remaining in the microchannels [39].

A suspension of cells was prepared at a cell concentration of 5×10^6 cells mL^{-1} and then introduced into a microchannel manually or by a syringe pump. Capillaries were then pinched by clips to stop the flow in the microchannel. The microfluidic device was wrapped with a wet lint-free wiper (BEMCOT™ M-1, Asahi Kasei, Tokyo, Japan) in plastic wrap to humidify the device. The microfluidic device was incubated at 37°C under an atmosphere of 5% CO_2 and 95% air for 5 h to allow cells to adhere to the bottom of the channel. The medium was then infused into the channel at 6.0 μL h^{-1} by the syringe pump placed outside the incubator (Fig. 1A and B) or the miniaturized infusion pump placed inside the incubator (Fig. 1C).

Shear stress during the culture was estimated as follows. Time-averaged shear stress τ in a rectangular microchannel is written as [40]:

$$\tau = \frac{2\mu Q}{wh^2}\left(\frac{m+1}{m}\right)(n+1) \quad (1)$$

where μ is the viscosity of the medium, Q is the volume flow rate, h is the height of the microchannel, w is the width of the microchannel, and m and n are empirical constants, with $m = 1.7 + 0.5(h/w)^{-1.4}$ and $n = 2$ for aspect ratios $h/w < 1/3$. As described previously [29], μ was assumed to be the same as that of water at 37°C, and estimated to be 7.0×10^{-3} g cm^{-1} s^{-1}. Using the μ value, a h of 67 μm, w of 300 μm, Q of 6.0 μL h^{-1} and Eq. 1, we obtained 0.061 dyn cm^{-2} as the time-averaged shear stress in the microchannel.

The miniaturized pump creates intermittent flow because of its peristaltic mechanism. Therefore, we measured instantaneous volume flow rate in a separate experiment and estimated shear stress (see Supporting information). The maximum instantaneous volume flow rate was 16.3 μL h^{-1}, and we obtained 0.17 dyn cm^{-2} as the maximum instantaneous shear stress.

The cultured cells were observed using an inverted microscope (IX71, Olympus, Tokyo, Japan) equipped with a CCD camera (Rolera XR, QImaging, Surrey, BC, Canada).

Phase-contrast images of HMEC-1 and HUVEC were taken at 102 h and 50 h, respectively, after introduction of the cell suspension.

2.5 Evaluation of proliferation rate

In macroscale experiments, 250 μL of a HMEC-1 suspension at a cell concentration of 4×10^5 cells mL^{-1} was added to 5 mL of fresh medium in a cell culture flask, and the cells were cultured under a static condition. In microscale experiments, microfluidic devices were degassed as described in the previous section. The medium was introduced into the microchannel at 1200 μL h^{-1} by a syringe pump. A suspension of HMEC-1 at a cell concentration of 5×10^6 cells mL^{-1} was then introduced into the microchannel at 600 μL h^{-1}, and the microfluidic devices were incubated in the CO_2 incubator for 4 h. Finally, the medium was pumped into the channel by the syringe pump or a miniaturized infusion pump at 6.0 μL h^{-1}. The cultured cells were observed as described in the previous section. Phase-contrast images of HMEC-1 were taken at 4 h (just before pumping medium), 28 h, 53 h, 83 h, 102 h, and 129 h after introduction of the cell suspension.

2.6 Evaluation of orientation

The orientation of HUVEC was evaluated in accordance with details provided in the literature [16]. Briefly, the angle of orientation was defined as the angle between the long axis of the cell and the direction of flow. Therefore, the angle of a cell that is completely oriented parallel to the microchannel is regarded as 0°, whereas the angle of a cell that is completely oriented perpendicular to the microchannel is regarded as 90°.

2.7 Immunofluorescent staining

HUVEC cultured in a microchannel were immunostained for Claudin-5, a transmembrane protein that is involved in tight junctions between endothelial cells [41]. After 50 h in culture, HUVEC was fixed with methanol, rinsed with PBS, blocked with PBS containing 1% BSA (Wako Pure Chemical Industries, Osaka, Japan) for 30 min, rinsed with PBS three times for 5 min each, and then reacted with 10 μg mL^{-1} anti-Claudin-5 antibody (ab53765, abcam, Cambridge, UK) for 12 h at 4°C. The cells were then rinsed with PBS three times for 5 min each, reacted with 6.7 μg mL^{-1} Alexa Fluor™ 555 goat anti-rabbit IgG antibody (A-21429, Invitrogen) for 30 min at room temperature, and rinsed with PBS three times for 5 min each. The nuclei of cells were counterstained with Dapi-Fluoromount-G™ (SouthernBiotech, Birmingham, AL, USA). Fluorescence images were taken using the same microscope described in Section 2.4 equipped with a 100-W high-pressure mercury lamp, a 20× objective lens (NA 0.40), and a cooled CCD camera (ORCA-R2, Hamamatsu Photonics, Hamamatsu, Japan). For Claudin-5 observation, a dichroic mirror block (U-MWIG3, excitation 530–550 nm and emission >575 nm) was used. For the observation of nuclei, another dichroic mirror block (U-MNUA2, excitation 360–370 nm and emission 420–460 nm) was used. The images were processed using image analysis software (Image J 1.45f, National Institutes of Health, MD, USA).

3 Results and discussions

3.1 Palmtop-sized microfluidic cell culture system

Figure 1D shows a photograph of the palmtop-sized microfluidic cell culture system. The system consists of a miniaturized infusion pump, a microfluidic device, a microtube, and tubes and capillaries that connect the components of the system. A reservoir (900 μL) of culture medium and an electrical control circuit are integrated into the pump (44 mm length, 22 mm width, 10 mm height, 7 g weight). The reservoir is connected to a rubber tube in the pump, and the tube is pushed by seven pins in the pump in a sequential manner. Therefore, the medium is pumped in a peristaltic manner. The range of volume flow rate is 1.0~30.0 μL h^{-1}. The pump is programmable, and we can configure up to ten discrete infusion steps. The pump is commercially available at low cost (¥25 000 per pump). The pump is disposable since it is an implantable pump for small laboratory animals, but should be reusable in our system if it is sterilized with appropriate solutions (e.g., 70% ethanol). In addition, the pump is powered by an internal battery, and therefore no cables or tubes are required from outside the system. As a result, the footprint of the whole system was reduced to 87 × 57 mm, which is, to the best of our knowledge, the smallest integrated cell culture system. The system can be placed in an incubator for culture and on a microscope for observation without detaching any electrical or fluidic connections from the system.

3.2 Culture of endothelial cells

Figure 2 shows typical images of HMEC-1 and HUVEC cultured in a microchannel. Both types of cells reached confluence in the microchannel, whether the channel was perfused by a syringe pump (Fig. 2A and C) or a miniaturized infusion pump (Fig. 2B and D). Therefore, both cell lines and normal cells reached confluence in the palmtop-sized cell culture system. HMEC-1 was not oriented to a specific direction, whereas HUVEC was oriented to the direction of the channel. The orientation of HUVEC is further discussed in Section 3.4.

We also observed air bubbles in the systems in some experiments. HMEC-1 was successfully cultured in the system shown in Fig. 1A. In contrast, when HUVEC was cultured in the system shown in Fig. 1A, air bubbles flowed into the channel and detached the cells from the surface of the channel (data not shown). Such issues were solved by placing

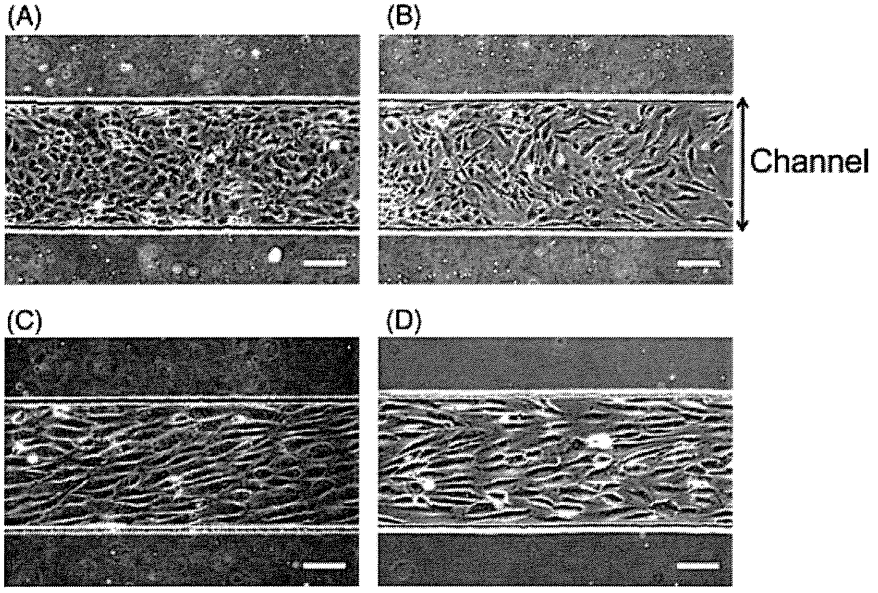

Figure 2. Phase-contrast images of (A, B) HMEC-1 and (C, D) HUVEC cultured in a microchannel. The cells were cultured with (A, C) a syringe pump and (B, D) a miniaturized infusion pump. Scale bar: 100 μm.

the bubble trap at the upstream point of the microchannel, as shown in Fig. 1B and C.

3.3 Growth rate of endothelial cells

Figure 3 shows the growth curve of HMEC-1 under three different culture procedures: static culture in a culture flask, perfusion culture in a microchannel with a syringe pump, and perfusion culture in a microchannel with a miniaturized infusion pump. In a culture flask, the cell density was 96 ± 28 cells mm^{-2} at the culture time of 4 h. The density then increased with time, and reached (1.4 ± 0.3) × 10^3 cells mm^{-2} at 102 h. Afterward, the density was almost constant, which meant the cells reached confluence at 102 h. In a microchannel perfused by a syringe pump, the cell density was (1.4 ± 0.4) × 10^2 cells mm^{-2} at 4 h and reached (1.1 ± 0.1) × 10^3 cells mm^{-2} at 102 h. In a microchannel perfused by a miniaturized infusion pump, the cell density was (1.5 ± 0.4) × 10^2 cells mm^{-2} at 4 h and reached (1.2 ± 0.1) × 10^3 cells mm^{-2} at 102 h. Clearly, the cell densities at the culture time of 4 h and 102 h in the aforementioned culture procedures were almost the same, and hence the proliferation rates of cells were also the same. Therefore, HMEC-1 cultured with the miniaturized infusion pump proliferated in a way similar to cells cultured with the syringe pump and in a culture flask.

3.4 Orientation

Figure 4 shows a histogram of the orientation angle of HUVEC under the different culture procedures. Under static culture in a culture flask, the orientation angle of HUVEC was random: the averaged orientation angle was 43.3 ± 25.1°,

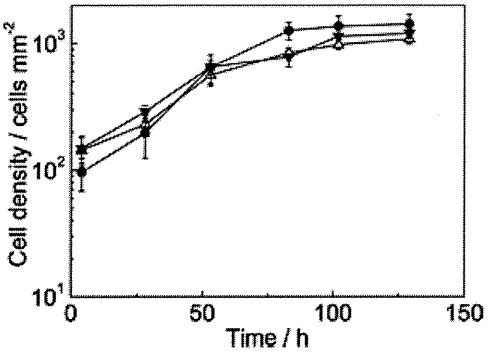

Figure 3. Growth curve of HMEC-1 under three different culture procedures: static culture in a culture flask (filled circles), perfusion culture in a microchannel with a syringe pump (open triangles), and perfusion culture in a microchannel with a miniaturized infusion pump (filled inverted triangles). The error bars indicate ±1SD of three experiments.

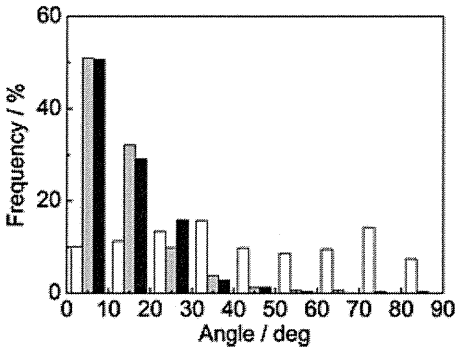

Figure 4. Histogram of orientation angle of HUVEC under three different culture procedures: static culture in a culture flask (white), perfusion culture in a microchannel with a syringe pump (gray), and perfusion culture in a microchannel with a miniaturized infusion pump (black). Culture time: 50 h. Data were taken from three experiments.

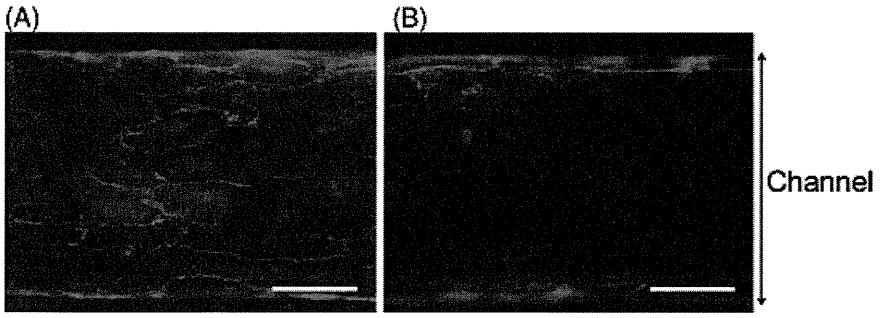

Figure 5. Immunofluorescence micrographs of HUVEC in a microchannel. Cells were immunostained for Claudin-5 (red, a marker of tight junctions). Nuclei of cells were counterstained with Dapi-Fluoromount-G (blue). (A) HUVEC cultured with a syringe pump. (B) HUVEC cultured with a miniaturized infusion pump. Scale bar: 100 μm.

which is close to the theoretical value of the averaged orientation angle for randomly oriented cells (45°). In contrast, the orientation angles of HUVEC cultured in microchannels were around zero: the averaged orientation angle of HUVEC cultured with a syringe pump and with a miniaturized infusion pump was 12.4 ± 12.0° and 12.1 ± 9.6°, respectively. Therefore, HUVEC was oriented to the direction along the channel. This result is consistent with previous reports concerning the orientation of HUVEC under continuous flow in a microchannel [13, 15].

3.5 Tight junctions

Tight junctions are a type of the intercellular junction, which represent the major transport pathway across the endothelium [42]. The presence of tight junctions between endothelial cells cultured in a microchannel has been demonstrated by TEER measurement [24]. However, the presence of tight junction proteins at the junctions has not been confirmed. Figure 5 shows immunofluorescence images of HUVEC in a microchannel. Claudin-5, the major transmembrane component of endothelial tight junctions, was localized along the cell peripheries as previously reported [43, 44], regardless of the type of pump used in the experiment. Therefore, the presence of tight junction proteins was confirmed with both types of pumps.

4 Concluding remarks

We have developed a palmtop-sized microfluidic cell culture system driven by a miniaturized infusion pump. Both HMEC-1 and HUVEC reached confluence in the system. HMEC-1 in the system proliferated with a rate similar to that of cells cultured with a syringe pump and in a culture flask. HUVEC was oriented in the microchannel regardless of the type of pump used in the experiment. The presence of tight junction proteins between the endothelial cells was, for the first time, directly confirmed by immunostaining of Claudin-5. We expect that the palmtop-sized microfluidic cell culture system is applicable to various cell types as a stand-alone and easy-to-use system for microfluidic bioanalysis.

The authors thank Prof. R. Shimada (Department of Mathematical and Physical Sciences, Faculty of Science, Japan Women's University) for her assistance with microfabrication. This work was partially supported by the JGC Corporation and JST CREST (Core Research for Evolutional Science & Technology).

The authors have declared no conflict of interest.

5 References

[1] Lenshof, A., Laurell, T., *Chem. Soc. Rev.* 2010, *39*, 1203–1217.

[2] Wu, M.-H., Huang, S.-B., Lee, G.-B., *Lab Chip* 2010, *10*, 939–956.

[3] Yamada, M., Kano, K., Tsuda, Y., Kobayashi, J., Yamato, M., Seki, M., Okano, T., *Biomed. Microdev.* 2007, *9*, 637–645.

[4] Petersson, F., Åberg, L., Swärd-Nilsson, A.-M., Laurell, T., *Anal. Chem.* 2007, *79*, 5117–5123.

[5] Hung, P. J., Lee, P. J., Sabounchi, P., Lin, R., Lee, L. P., *Biotechnol. Bioeng.* 2005, *89*, 1–8.

[6] Young, E. W. K., Simmons, C. A., *Lab Chip* 2010, *10*, 143–160.

[7] Fidkowski, C., Kaazempur-Mofrad, M. R., Borenstein, J., Vacanti, J. P., Langer, R., Wang, Y., *Tissue Eng.* 2005, *11*, 302–309.

[8] Golden, A. P., Tien, J., *Lab Chip* 2007, *7*, 720–725.

[9] Shin, M., Matsuda, K., Ishii, O., Terai, H., Kaazempur-Mofrad, M., Borenstein, J., Detmar, M., Vacanti, J. P., *Biomed. Microdev.* 2004, *6*, 269–278.

[10] Lindström, S., Mori, K., Ohashi, T., Andersson-Svahn, H., *Electrophoresis* 2009, *30*, 4166–4171.

[11] Chrobak, K. M., Potter, D. R., Tien, J., *Microvasc. Res.* 2006, *71*, 185–196.

[12] Song, J. W., Cavnar, S. P., Walker, A. C., Luker, K. E., Gupta, M., Tung, Y.-C., Luker, G. D., Takayama, S., *PLoS ONE* 2009, *4*, e5756.

[13] Tkachenko, E., Gutierrez, E., Ginsberg, M. H., Groisman, A., *Lab Chip* 2009, *9*, 1085–1095.

[14] Chau, L., Doran, M., Cooper-White, J., *Lab Chip* 2009, *9*, 1897–1902.

[15] van der Meer, A. D., Poot, A. A., Feijen, J., Vermes, I., *Biomicrofluidics* 2010, *4*, 011103.

[16] Shao, J., Wu, L., Wu, J., Zheng, Y., Zhao, H., Jin, Q., Zhao, J., *Lab Chip* 2009, *9*, 3118–3125.

[17] Chin, L. K., Yu, J. Q., Fu, Y., Yu, T., Liu, A. Q., Luo, K. Q., *Lab Chip* 2011, *11*, 1856–1863.

[18] Song, J. W., Gu, W., Futai, N., Warner, K. A., Nor, J. E., Takayama, S., *Anal. Chem.* 2005, *77*, 3993–3999.

[19] Nalayanda, D. D., Puleo, C. M., Fulton, W. B., Wang, T. H., Abdullah, F., *Exp. Lung Res.* 2007, *33*, 321–335.

[20] Nalayanda, D. D., Wang, Q., Fulton, W. B., Wang, T.-H., Abdullah, F., *J. Pediatr. Surg.* 2010, *45*, 45–51.

[21] Esch, M. B., Post, D. J., Shuler, M. L., Stokol, T., *Tissue Eng. A* 2011, *17*, 2965–2971.

[22] Huh, D., Matthews, B. D., Mammoto, A., Montoya-Zavala, M., Hsin, H. Y., Ingber, D. E., *Science* 2010, *328*, 1662–1668.

[23] Young, E. W. K., Watson, M. W. L., Srigunapalan, S., Wheeler, A. R., Simmons, C. A., *Anal. Chem.* 2010, *82*, 808–816.

[24] Douville, N. J., Tung, Y.-C., Li, R., Wang, J. D., El-Sayed, M. E. H., Takayama, S., *Anal. Chem.* 2010, *82*, 2505–2511.

[25] Vogel, P. A., Halpin, S. T., Martin, R. S., Spence, D. M., *Anal. Chem.* 2011, *83*, 4296–4301.

[26] Leclerc, E., David, B., Griscom, L., Lepioufle, B., Fujii, T., Layrolle, P., Legallaisa, C., *Biomaterials* 2006, *27*, 586–595.

[27] Kou, S., Pan, L., van Noort, D., Meng, G., Wu, X., Sun, H., Xu, J., Lee, I., *Biochem. Biophys. Res. Commun.* 2011, *408*, 350–355.

[28] Sato, K., Mawatari, K., Kitamori, T., *Lab Chip* 2008, *8*, 1992–1998.

[29] Tanaka, Y., Kikukawa, Y., Sato, K., Sugii, Y., Kitamori, T., *Anal. Sci.* 2007, *23*, 261–266.

[30] Yamashita, T., Tanaka, Y., Idota, N., Sato, K., Mawatari, K., Kitamori, T., *Biomaterials* 2011, *32*, 2459–2465.

[31] Jang, K., Sato, K., Igawa, K., Chung, U.-I., Kitamori, T., *Anal. Bioanal. Chem.* 2008, *390*, 825–832.

[32] Herricks, T., Seydel, K. B., Turner, G., Molyneux, M., Heyderman, R., Taylor, T., Rathod, P. K., *Lab Chip* 2011, *11*, 2994–3000.

[33] Bowen, A. L., Martin, R. S., *Electrophoresis* 2010, *31*, 2534–2540.

[34] Gómez-Sjöberg, R., Leyrat, A. A., Pirone, D. M., Chen, C. S., Quake, S. R., *Anal. Chem.* 2007, *79*, 8557–8563.

[35] Futai, N., Gu, W., Song, J. W., Takayama, S., *Lab Chip* 2006, *6*, 149–154.

[36] Ades, E. W., Candal, F. J., Swerlick, R. A., George, V. G., Summers, S., Bosse, D. C., Lawley, T. J., *J. Invest. Dermatol.* 1992, *99*, 683–690.

[37] Hosokawa, K., Fujii, T., Endo, I., *Anal. Chem.* 1999, *71*, 4781–4785.

[38] Imura, Y., Asano, Y., Sato, K., Yoshimura, E., *Anal. Sci.* 2009, *25*, 1403–1407.

[39] Hosokawa, K., Sato, K., Ichikawa, N., Maeda, M., *Lab Chip* 2004, *4*, 181–185.

[40] Young, E. W., Simmons, C. A., *Lab Chip* 2010, *10*, 143–160.

[41] Morita, K., Sasaki, H., Furuse, M., Tsukita, S., *J. Cell Biol.* 1999, *147*, 185–194.

[42] Tarbell, J. M., *Cardiovasc. Res.* 2010, *87*, 320–330.

[43] Rodewald, M., Herr, D., Duncan, W. C., Fraser, H. M., Hack, G., Konrad, R., Gagsteiger, F., Kreienberg, R., Wulff, C., *Human Reprod.* 2009, *24*, 1191–1199.

[44] Beese, M., Wyss, K., Haubitz, M., Kirsch, T., *BMC Cell Biol.* 2010, *11*, 68.

Open

Oncogene (2013), 1–10

www.nature.com/onc

ORIGINAL ARTICLE

Involvement of EphA2-mediated tyrosine phosphorylation of Shp2 in Shp2-regulated activation of extracellular signal-regulated kinase

K Miura[1], Y Wakayama[1], M Tanino[2], Y Orba[3], H Sawa[3], M Hatakeyama[4], S Tanaka[2], H Sabe[5] and N Mochizuki[1]

Shp2 is a positive regulator for Erk activation downstream of receptor tyrosine kinases for growth factors. It has been controversial how Shp2 induces Erk activation. We here demonstrate that EphA2 is responsible for Shp2-mediated Erk activation by phosphorylating Tyr542 and Tyr580 of Shp2 in the cells stimulated with growth factors. In NMuMG mammary epithelial cells stimulated with hepatocyte growth factor (HGF), HGF-dependent Erk phosphorylation was prolonged only in the presence of EphA2. This Erk activation paralleled the phosphorylation of Tyr542/580 of Shp2 and the association of Grb2 with Shp2, suggesting the positive signal involving Grb2 signal to activate Ras-Erk pathway. Immunohistochemical studies of mammary cancer specimens revealed that the cancer progression was associated with both Tyr580 phosphorylation of Shp2 and increased expression of EphA2, which were also correlated with increased Erk phosphorylation. Overexpression of either Shp2Thr468Met (a phosphatase-defective mutant found in *L*entigines, *E*lectrocardiographic abnormalities, *O*cular hypertelorism, *P*ulmonary stenosis, *A*bnormal genitalia, *R*etardation of growth and sensorineural *D*eafness (LEOPARD) syndrome) or Shp2Asn308Asp (a phosphatase-active mutant found in Noonan syndrome) with EphA2 exhibited comparable activation of Erk and stronger activation than wild-type Shp2, suggesting the phosphatase-independent Erk activation. Expression of Shp2Thr468Met with Tyr542/580Phe mutations resulted in the suppression of Erk activation. Phosphatase-active and -inactive, and wild-type Shp2s bound equally to Grb2, suggesting that phosphorylation of Tyr542/580 of Shp2 was essential but not sufficient for Shp2-mediated Erk activation. We found that Gab1 (Grb2-associated binder 1) was involved in the mutant Shp2-mediated Erk activation. Zebrafish injected with Shp2Thr468Met mRNA showed cardiac edema, whereas those depleted of EphA2b showed less phenotype, suggesting that EphA2 might partly account for the phenotype of LEOPARD syndrome. Collectively, tyrosine phosphorylation of Shp2 by EphA2 contributes to the phosphatase-independent Shp2-mediated activation of Erk and might be involved in Shp2-associated diseases.

Oncogene advance online publication, 14 January 2013; doi:10.1038/onc.2012.571

Keywords: Shp2; EphA2; Erk; cancer; LEOPARD syndrome

INTRODUCTION

Shp2, encoded by the *PTPN11* gene, is a protein tyrosine phosphatase that acts as a positive regulator of Ras-Erk pathway.[1–3] Shp2 contains two tandem Src homology 2 (SH2) domains, a protein tyrosine phosphatase domain and tyrosine phosphorylation sites.[1–3] Shp2 is thought to be inactive by forming intramolecular folding under unstimulated conditions, whereas it becomes active when the amino-terminal SH2 domains bind to phosphorylated molecules, including Grb2-associated binder (Gab), insulin receptor substrate and fibroblast growth factor receptor substrate, by forming an open conformation.[2,3] It remains unclear how Shp2 is involved in the activation of Erk signal and whether its phosphatase activity of Shp2 is essential for the activation of Ras-Erk signal. Phosphatase-active mutation of Shp2 (a genetic mutation of *PTPN11* encoding Asn308Asp, hereafter referred to as N308D) is found in patients with Noonan syndrome, whereas phosphatase-defective mutation (Thr468Met, hereafter referred to as T468M) is found in those with *L*entigines, *E*lectrocardiographic abnormalities, *O*cular hypertelorism, *P*ulmonary stenosis, *A*bnormal genitalia, *R*etardation of growth and sensorineural *D*eafness (LEOPARD) syndrome.[4,5] The patients with Noonan syndrome and those with LEOPARD syndrome exhibit the overlapping symptoms, including craniofacial abnormalities, cardiac defects and growth retardation. In addition, leukemia diseases are often found in the patients with those syndromes.[4,5] Cardiomyocytes derived from induced pluripotent stem cells from the patient with LEOPARD syndrome show an increased activation of Erk,[6] suggesting the phosphatase-independent role of Shp2 in the Erk activation.

Growth factors promote cell proliferation *via* their specific tyrosine kinase receptors by activating Ras-Erk signaling. Autophosphorylated tyrosine kinase receptors provide the binding sites for adaptor molecules containing SH2 domain and for scaffold adaptor molecules to activate Sos-Ras-Erk signaling pathway.

[1]Department of Cell Biology, National Cerebral and Cardiovascular Center Research Institute, Suita, Osaka, Japan; [2]Laboratory of Cancer Research, Department of Pathology, Hokkaido University, Graduate School of Medicine, Kita-ku, Sapporo, Japan; [3]Department of Molecular Pathobiology, Hokkaido University Research Center for Zoonosis Control, Sapporo, Japan; [4]Division of Microbiology, Graduate School of Medicine, University of Tokyo, Bunkyo-ku, Tokyo, Japan and [5]Department of Molecular Biology, Hokkaido University, Graduate School of Medicine, Kita-ku, Sapporo, Japan. Correspondence: Dr K Miura, Department of Cell Biology, National Cerebral and Cardiovascular Center Research Institute, 5-7-1 Fujishirodai, Suita, Osaka 565-8565, Japan. or Naoki Mochizuki, Department of Cell Biology, National Cerebral and Cardiovascular Center Research Institute, 5-7-1 Fujishirodai, Suita, Osaka 565-8565, Japan.
E-mail: miurako@ri.ncvc.go.jp or nmochizu@ri.ncvc.go.jp
Received 5 April 2012; revised 26 October 2012; accepted 26 October 2012

Although the Ras-Erk activation is transient, Shp2 is reported to be a modulator that prolongs the activation of Erk.[7] Hepatocyte growth factor (HGF) induces phosphorylation of Met receptor and subsequent recruitment of an adaptor scaffolding protein, Gab1. Furthermore, phosphorylated Gab1 becomes associated with SH2 domains of Shp2.[1–3] This association of Shp2 with Gab1 leads to the Ras-Erk activation.[1–3] In addition, it has been suggested that the phosphorylated Tyr542 and Tyr580 recruit Grb2/Sos complex to activate Ras-Erk signaling.[2,7,8] Recently, it was reported that ZAP70, a non-receptor tyrosine kinase, enhances phosphorylation of Shp2 at Tyr580 and activates Erk.[9] However, it is still unclear how growth factor stimuli induce tyrosine phosphorylation of Shp2.

Activation of Ras-Erk signaling pathway is observed in cancer progression as well as in the diseases called 'Rasopathies', including Noonan syndrome, LEOPARD syndrome, Costello syndrome and neurofibromatosis type 1.[4,5] The diseases with genetic mutations of the genes encoding the molecules constituting the Ras-Erk signaling pathway, such as SOS1, KRAS, HRAS, NRAS, RAF1, BRAF, PTPN11, MEK1/2, SHOC2, CBL, SPREAD1 and NF1, are also included in Rasopathies. Active mutations of receptor tyrosine kinases for growth factors inducing Ras-Erk activation, such as EGFR, ErbB2, FGFR and c-KIT, are found in patients with a wide variety of cancers,[10] suggesting the significant role of the Erk signal in cancer promotion. Furthermore, the overexpression and the contribution to Erk activation of another receptor tyrosine kinase, EphA2, have been reported in many types of cancers.[11,12]

EphA2 is a member of the EphA family of receptor tyrosine kinases consisting of nine EphAs (EphA1–A8 and A10) for membrane-anchored ephrinA ligands.[13,14] Paradoxically, EphA2 has both tumor-promoting and -suppressing roles. EphrinA ligands suppress the cell proliferation via activation of EphA2, whereas extracellular growth factors promote cell proliferation by an indirect activation of EphA2 through their tyrosine kinase receptor activation.[13,14] However, the molecular mechanisms by which EphA2 promotes the Ras-Erk pathway without the engagement of ephrinA are unknown. We report here that EphA2 phosphorylates Tyr542/580 of Shp2, subsequently recruiting Grb2 to activate Erk, and that Gab1 might function in Shp2T468M-dependent Erk activation besides or cooperatively phosphorylated Shp2/Grb2-mediated signaling. Moreover, we demonstrate the possible role for this Shp2-mediated Erk activation signal in cancer progression and in LEOPARD syndrome.

RESULTS

EphA2 is required for HGF-induced prolonged and/or enhanced activation of Erk

Shp2 is involved in the activation of the Ras-Erk pathway by growth factor signaling.[1,3] To confirm that Shp2 is required for the HGF-mediated activation of Erk in epithelial NMuMG cells, we examined the degree and duration of Erk activation of the cells stimulated with HGF. When NMuMG cells were stimulated with HGF, phosphorylation of Erk peaked at 15 min after the stimulation and continued for 180 min (Figures 1a and b). When those depleted of Shp2 were stimulated with HGF, the peak Erk phosphorylation was reduced (Figures 1a and b). In addition to the reduction of peak activation of Erk, the dephosphorylation of Erk after the peak was faster than the control cells, indicating the role for Shp2 in the enhancement and the prolongation of Erk phosphorylation in NMuMG cells upon HGF stimulation (Figures 1a and b). We wondered how Shp2 is involved in the regulation of Erk activation in the cells stimulated with HGF. Previously, phosphorylation of Tyr542 and Tyr580 is reported to be important for Shp2-mediated Erk activation,[7] although the kinases that phosphorylate these tyrosine residues have not been identified. Growth factor receptor simulation is thought to activate not only their receptors but also other signaling pathway, including EphA2.[14] Therefore, we hypothesized that EphA2 might be responsible for HGF-induced Erk activation signal involving Shp2.

To test the requirement of EphA2 for HGF-induced prolonged and enhanced activation of Erk, we studied the effect of depletion of EphA2 on the HGF-induced Erk activation in NMuMG cells. Knockdown of EphA2 resulted in shortened Erk activation and reduced phosphorylation of Tyr542/580 of Shp2, which was required for recruitment of Grb2 (Figures 1c and d). Consistently, the association of Shp2 with Grb2 was reduced in the cells depleted of EphA2 (Figure 1c), suggesting that EphA2 is required for phosphorylation of Shp2 and Shp2-dependent prolonged and enhanced activation of Erk. To further investigate whether EphA2 is involved in Erk activation in other types of cells stimulated with growth factors, we examined the fibroblast growth factor 2-stimulated human umbilical vein endothelial cells and HGF-stimulated C6 glioma cells. In both cells, knockdown of EphA2 led to attenuation of Erk activation and reduction of Grb2 binding to phosphorylated Shp2 (Figures 1e–h). These results indicate the common signaling pathway that involves EphA2-regulated phosphorylation of Shp2 in Erk activation of the cells stimulated with the growth factors. To understand the consequence of prolonged Erk activation mediated by EphA2 and Shp2, we analyzed the proliferation of NMuMG cells stimulated with HGF. The cell number of those depleted of either EhpA2 or Shp2 cultured for a few days in the presence of HGF was half of the control cells, indicating the essential role of EphA2 and Shp2 in HGF-dependent cell proliferation (Figure 1i).

To further confirm the contribution of EphA2 to the Shp2-mediated Erk activation, we compared two cell lines: NMuMG cells and HEK 293T cells, both of which express similar amount of Met and Shp2, although NMuMG cells express EphA2 more than HEK293T cells (Figure 2a). The extent of Erk activation in NMuMG cells was much greater than that in HEK293T cells when those cells

Figure 1. Contribution of EphA2-dependent phosphorylation of Shp2 to the growth factor-induced Erk activation. (**a**) Immunoblot analyses with the antibodies indicated at the left using the cell lysates prepared from the NMuMG cells pretreated with short interfering RNAs (siRNAs) indicated on the top and stimulated with HGF for the time indicated on the top. (**b**) Quantitative analyses of Erk phosphorylation by HGF in cells treated with control siRNA (control, closed circle) or siRNA against Shp2 (siShp2, open circle). Fold induction after the HGF stimulation was plotted as the value of the intensity of phosphorylated (p)-Erk divided by that of Erk (0 min) was 1. Experiments were performed at least three times. Data are represented as mean with s.d. $*P<0.05$ between the cells treated with control and those treated with siShp2. (**c**) Immunoblot analyses with the antibodies indicated at the left using the cell lysates (Total) or the immunoprecipitates with anti-Shp2 (IP: Shp2) prepared from NMuMG cells pretreated with sRNAs indicated on the top and stimulated with HGF for the time indicated on the top. (**d**) Phosphorylation of Erk observed in (**c**) was quantified as described in the legend for (**b**). (**e**) and (**g**) Immunoblot analyses with the antibodies indicated at the left using the cell lysates of human umbilical vein endothelial cells (HUVECs) stimulated with fibroblast growth factor-2 (FGF-2) (**e**) and those of C6 glioma cells stimulated with HGF (**g**) as described in the legend of (**b**). (**f**) and (**h**) Phosphorylation of Erk observed in (**e**) and (**g**) was quantified, respectively, as described in the legend of (**b**). (**i**) The number of NMuMG cells treated with either control siRNA (white), EphA2 siRNA (black) or Shp2 siRNA (gray) and cultured in the presence or absence of HGF was counted. The cells transfected for 24 h with siRNAs were replated at the density of 2×10^4 per well in the 12-well plate and were subjected to the calculation at the time after being replated as indicated at the bottom. Data are represented as mean of at least three independent experiments with s.d. $*P<0.05$ between the cells treated with control and those treated with either EphA2 siRNA or Shp2 siRNA.

were stimulated with HGF (Figure 2a). Furthermore, HGF-dependent phosphorylation of Tyr542 was found in NMuMG cells but not in HEK293T cells. These results raise the possibility that the expression of EphA2 might determine the duration and amplitude of Erk activation, because expression of both Met and Shp2 are comparable between the two cell lines. To test this, we expressed

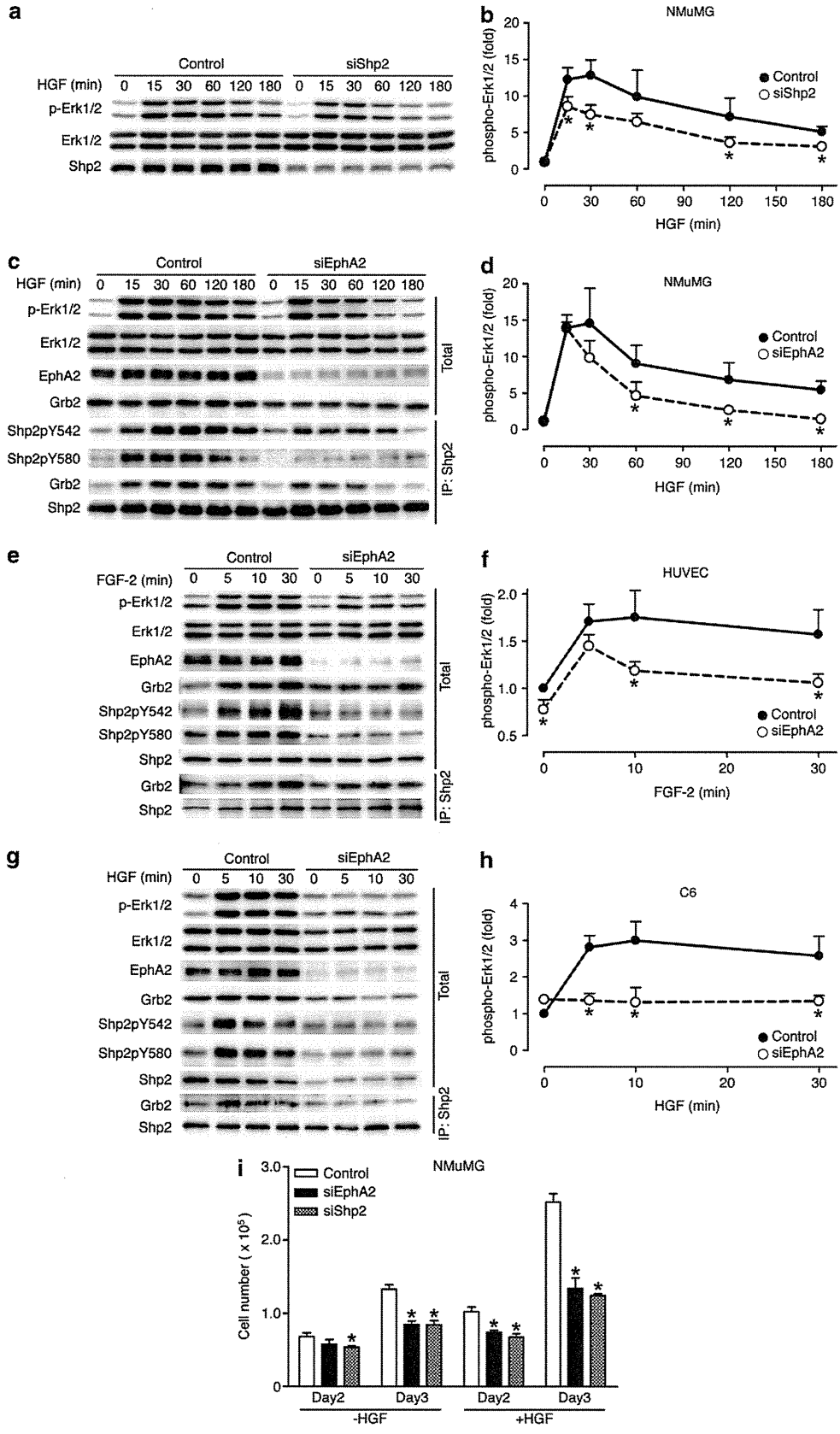

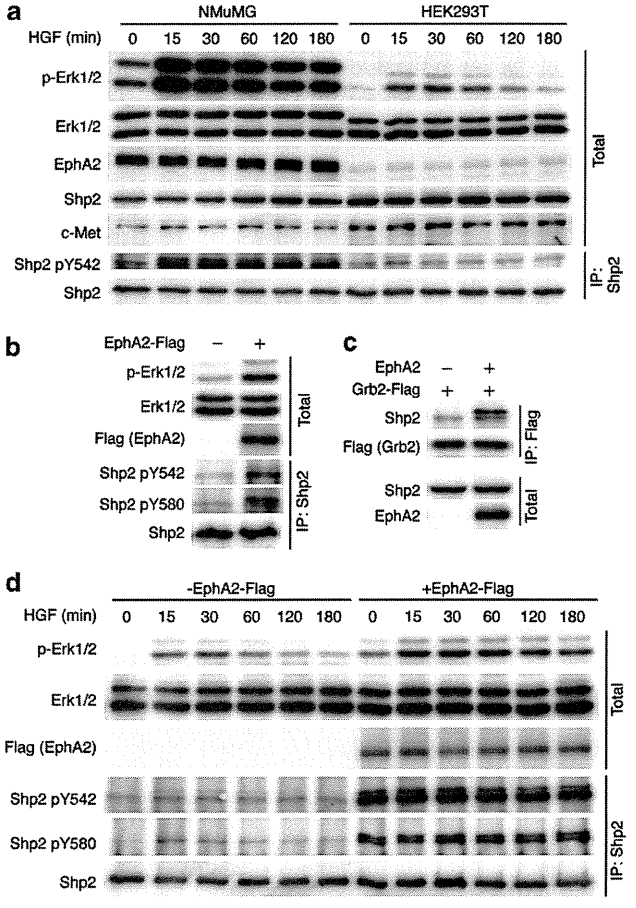

Figure 2. EphA2 can regulate Erk activation through the phosphorylation of Shp2 and the association of Shp2 with Grb2. (**a**) Immunoblot analyses with the antibodies indicated at the left using the cell lysates (Total) or the immunoprecipitates with anti-Shp2 (IP: Shp2) prepared from NMuMG (left panel) and HEK293Tcells (right panel) stimulated with HGF (20 ng/ml) for the time indicated on the top. (**b**) Immunoblot analyses with the antibodies indicated at the left using the cell lysates (Total) or the immunoprecipitates with anti-Shp2 (IP: Shp2) prepared from HEK293T cells tranfected with the plasmids indicated on the top. (**c**) Immunoblot analyses with the antibodies indicated at the left using the cell lysates (Total) or the immunoprecipitates with anti-Flag (IP: Flag) prepared from HEK293T cells transfected with the plasmids indicated on the top. (**d**) Immunoblot analyses with the antibodies indicated at the left using the cell lysates (Total) or the immunoprecipitates with anti-Shp2 (IP: Shp2) prepared from HEK293T cells transfected with plasmids indicated on the top and stimulated with HGF for the time indicated on the top. (**a–d**) Each result is the representative of at least three independent experiments.

EphA2 in HEK293T cells and examined the phosphorylation of Shp2, the association of Shp2 with Grb2 and the Erk activation upon HGF stimulation. Forced expression of EphA2 in the cells resulted in the phosphorylation of Tyr542/580 of Shp2 and the association of Shp2 with Grb2 (Figures 2b and c). Furthermore, the HGF-dependent Erk activation was significantly enhanced in the cells expressing EphA2 (Figure 2d), suggesting the contribution of EphA2 to growth factor-induced enhancement and prolongation of Erk activation.

Shp2 phosphorylation-dependent Erk activation irrespective of its phosphatase activity

Phosphatase-active mutant of Shp2 (N308D) and phosphatase-defective mutant of Shp2 (T468M) cause Noonan syndrome and LEOPARD syndrome, respectively (Figure 3a).[5,15] To examine the effect of EphA2 on the Erk activation in the cells expressing these Shp2 mutants, we expressed Shp2 mutants with EphA2. The cells expressing either wild-type Shp2 or mutant Shp2 (T468M or N308D) showed the similar degree of phosphorylation on Tyr542/580, whereas Erk activation was weaker in those expressing wild-type than those expressing mutant Shp2 (Figure 3b). Of note, there was no difference in the Erk activation between the cells expressing Shp2T468M and those expressing Shp2N308D (Figure 3b). These data suggest the phosphatase-independent mechanism underlying Shp2-mediated Erk activation.

There was no difference in the association of mutant Shp2 (T468M or N308D) and wild-type Shp2 with Grb2 (Figure 3c), indicating that the association of Shp2 with Grb2 is not sufficient to induce Erk activation, because the activation of Erk in the cells expressing either Shp2T468M or Shp2N308D with EphA2 was greater than those expressing wild-type Shp2 with EphA2 (Figure 3b). However, the Erk activation in the cells expressing EphA2 and Shp2T468M was greater than those expressing EphA2 and Shp2T468M with mutations on both Tyr542 and Tyr580 (Shp2T468M/2YF) (Figure 3d), indicating that phosphorylation of Tyr542/580 is required for EphA2 in Shp2-mediated Erk activation. Consistently, Shp2T468M/2YF mutant could not associate with Grb2 even in the cells expressing EphA2 (Figure 3e). Furthermore, we found that Grb2 with SH3 mutation (either P49L or G203R) but not that with SH2 mutation (R86K) could bind to Shp2T468M (Figure 3f), indicating that the association of Shp2 with Grb2 is mediated by the phosphorylation of Tyr542 and Tyr580 of Shp2 and the SH2 domain of Grb2. Overexpression of a dominant-negative form of Grb2, Grb2P49L, significantly reduced EphA2-dependent Shp2T468-mediated Erk phosphorylation (Figure 3g and Supplementary Figure S1), although it did not completely block it, suggesting the contribution of Grb2 to this Erk activation signal and implying the alternative signaling independent of Grb2.

To understand the molecular mechanism underlying the difference in the degree of Erk activation between the cells expressing wild type and those expressing Shp2T468M, we examined the role of Gab1 in Shp2-mediated Erk activation, because the complex of Gab1 and Shp2 is reported to be essential for growth factor-induced Erk activation. Tyr627 of Gab1 is essential for the binding of Shp2 to Gab1.[16] We found that Tyr627 was less phosphorylated in the cells expressing wild-type Shp2 than those expressing either Shp2T468M or Shp2N308D (Figure 3h). Furthermore, a dominant-negative mutant Gab1 (Gab1Y627F) incapable of being phosphorylated inhibited the EphA2-dependent Shp2T468M-mediated Erk phosphorylation, although phosphorylation of Tyr542/580 of Shp2T468M was preserved (Figure 3i). Collectively, these data suggest that phosphorylation of Tyr542/580, which recruits Grb2, is required but not sufficient for EphA2-dependent Shp2T468M-mediated Erk activation.

Requirement of tyrosine phosphorylation of Shp2 and dispensability of phosphatase activity of Shp2 for the Erk activation in the cells expressing Shp2 and EphA2

To test both the requirement of phosphorylation of Tyr542/580 and the dispensability of phosphatase activity of Shp2 in the cells stimulated with HGF, we examined the Erk activation in HEK293 cells expressing Shp2T468M and in those expressing Shp2T468M/2YF or wild-type Shp2 when stimulated with HGF. Even in the cells without forced expression of EphA2, the cells expressing Shp2T468M exhibited greater Erk activation than those expressing either Shp2T468M/2YF or wild-type Shp2 in response to HGF (Figure 4a), although the Erk activation in the cells expressing Shp2T468M/2YF was greater than that in the cells expressing wild-type Shp2 (Figure 4c). Increase in phosphorylation of Tyr542/580 even in the cells expressing Shp2T468M and wild-type Shp2 was subtle compared with cells without forced expression of Shp2

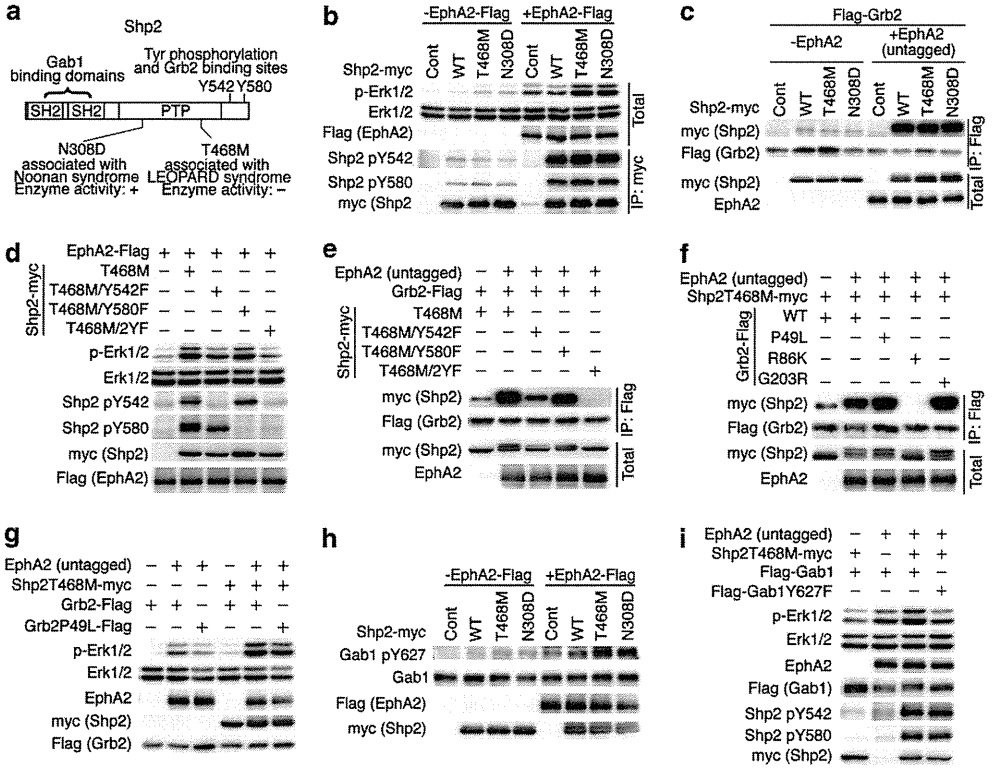

Figure 3. EphA2 and disease-associated Shp2 mutants synergistically enhance basal Erk activity in HEK293T cells. (**a**) Schematic illustration of the domain structure of Shp2 and the amino-acid residues that we examined in this study. SH2, Src homology 2 domain; PTP, protein tyrosine phosphatase domain. (**b**) Immunoblot analyses with the antibodies indicated at the left using the cell lysates (Total) or the immunoprecipitates with anti-myc (IP: myc) prepared from HEK293T cells transfected with the plasmids indicated on the top. (**c**) Immunoblot analyses with the antibodies indicated at the left using the cell lysates (Total) or the immunoprecipitates with anti-Flag (IP: Flag) prepared from HEK293T cells transfected with the plasmids indicated on the top. (**d**) Immunoblot analyses with the antibodies indicated at the left using the cell lysates prepared from HEK293T cells transfected with the plasmids indicated on the top. (**e** and **f**) Immunoblot analyses with the antibodies indicated at the left using the cell lysates (Total) or the immunoprecipitates with anti-Flag (IP: Flag) prepared from HEK293T cells transfected with the plasmids indicated on the top. (**g**–**i**) Immunoblot analyses with the antibodies indicated at the left using the cell lysates prepared from HEK293T cells transfected with the plasmids indicated on the top. (**b**–**i**) Each result is the representative of the three independent experiments.

(Figure 4a). Notably, the Erk activation in the cells expressing Shp2T468M was decreased within 120 min (Figure 4c).

In clear contrast to the cells without forced expression of EphA2, the Erk activation in the cells expressing EphA2 with Shp2T468M was prolonged even 120 min after the stimulation with HGF (Figures 4b and d and Supplementary Figure S2). There was no EphA2-dependent enhancement or prolongation of Erk activation among the cells without forced expression of Shp2, those expressing Shp2T468M/2YF and those expressing wild-type Shp2 (Figures 4b and d). These data suggest that HGF-induced prolonged activation of Erk involving Shp2 does not need Shp2 phosphatase activity but tyrosine phosphorylation of Shp2.

We examined the Gab1 phosphorylation to understand the difference of Erk phosphorylation among Shp2T468M, Shp2T468M/2YF and wild-type Shp2 in HEK293T cells and those overexpressing EphA2. Tyr627 phosphorylation of Gab1 in the cells expressing Shp2T468M/2YF was weaker than those expressing Shp2T468M and stronger than those expressing wild-type Shp2 in both cells (Supplementary Figure S3), suggesting the role for Gab1 in Shp2T468M-mediated Erk activation.

Tyrosine kinase activity of EphA2 is required for phosphorylation of Shp2 and Erk activation by Shp2

To examine how EphA2 phosphorylates Shp2, we studied the effects of mutated EphA2 on Shp2T468M-dependent Erk activation in HEK293T cells. We found that the Erk activation and the phosphorylation of Tyr542/580 of Shp2 was abolished in the cells expressing EphA2K646M, which lacks the kinase activity[17] (Figure 5a). Recently, the phosphorylation of Ser897 by Akt was reported to be important for cancer cell migration.[18] The replacement of Ser897 with Ala did not affect the Erk activation (Figure 5a). Besides these, EphA2 has multiple tyrosine phosphorylation sites (Tyr588, Tyr594 and Tyr772) important for its tyrosine kinase activity and for recruiting SH2 domain-containing molecules.[19] The cells expressing either EphA2Y588F or Y772F exhibited less Shp2T468M-dependent Erk activation and phosphorylation of Shp2T468M than those expressing wild-type EphA2 (Figure 5a). These data suggest that the kinase activity of EphA2 is essential for Shp2 phosphorylation and that the additional molecules downstream of EphA2 might modify the phosphorylation of Shp2. To further confirm the importance of tyrosine kinase activity, we examined the effect of Dasatinib, a potent inhibitor for EphA2, on the activation of Erk and on the phosphorylation of Shp2.[20] Treatment of the cells expressing Shp2T468M and EphA2 with Dasatinib resulted in a rapid decrease in Erk phosphorylation as well as in the phosphorylation of Shp2 and EphA2 (Figures 5b and c). We finally examined whether EphA2 directly phosphorylates Shp2 *in vitro* using purified EphA2 and Shp2. EphA2 phosphorylated Tyr542 and Tyr580 of Shp2 (Figure 5d). These results indicate the importance of tyrosine kinase activity of EphA2 in the phosphorylation of Shp2.

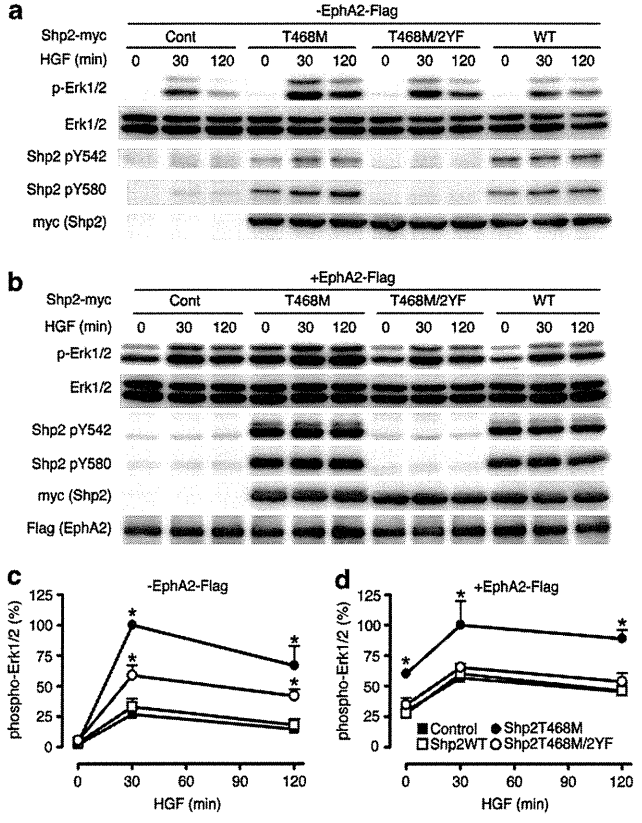

Figure 4. Phosphatase-independent and EphA2-dependent Erk activation in Shp2-mediated signal. (**a** and **b**) Immunoblot analyses with the antibodies indicated at the left using the cell lysates prepared from HEK293T cells transfected with the plasmids indicated on the top and stimulated with HGF for the time indicated on the top. (**c** and **d**) Quantitative analyses of phosphorylation of Erk by HGF in cells expressing empty vector (closed square), Shp2WT-myc, (open square), Shp2T468M-myc (closed circle) or Shp2T468M/2YF (open circle). The relative phosphorylation of Erk was calculated as the value of the intensity of phosphorylated (p)-Erk divided by that of Erk at 30 min in cells transfected with Shp2T468M was 100%. Experiments were performed at least three times. Data are represented as mean with s.d. $*P<0.05$ among the four groups.

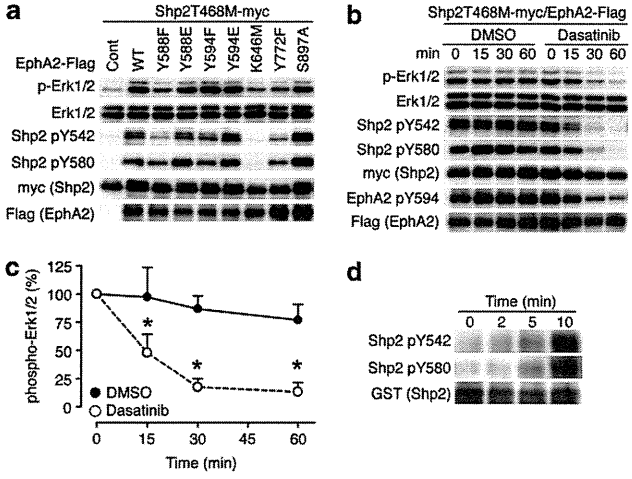

Figure 5. Tyrosine kinase activity of EphA2 is required for phosphorylation of Shp2 and Erk activation by Shp2. (**a**) Immunoblot analyses with the antibodies indicated at the left using the cell lysates prepared from HEK293T cells transfected with the plasmids indicated on the top. A representative result of three independent experiments. (**b**) Immunoblot analyses with the antibodies indicated at the left using the cell lysates prepared from HEK293T cells transfected with the plasmids indicated on the top and treated with Dasatinib (100 nM) or dimethylsulfoxide (DMSO) for the time indicated on the top. (**c**) Quantitative analysis of (**b**). The relative Erk phosphorylation after the treatment with Dasatinib was calculated as the intensity of p-Erk divided by that of Erk from the untreated cells at the 0 min was 100%. Data are represented as mean with s.d. $*P<0.05$ between the cells treated with DMSO and those treated with Dasatinib. (**d**) Immunoblot analyses with the antibodies indicated at the left using GST-Shp2 incubated with GST-EphA2 for the time indicated on the top.

Phosphorylation of Shp2 and Erk in breast cancer-expressing EphA2

We then tried to test whether the signal, EphA2-mediated phosphorylation of Shp2 and subsequent Erk activation, is involved in diseases. EphA2 is often overexpressed in a variety of malignant cancers, including breast, lung, prostate and colon cancers.[11] We, therefore, hypothesized that the phosphorylation of Shp2 is enhanced by EphA2 in cancer. To test this hypothesis, we performed immunohistochemical analyses of human breast cancer tissues to investigate the relevance of EphA2 expression to the phosphorylation of Shp2. In normal mammary glands, neither EphA2 nor phosphorylation of Shp2 at Tyr580 was detected (Figure 6a). However, in the ductal carcinoma *in situ* and in the invasive breast cancer, the expression of EphA2 and the phosphorylation of Shp2 at Tyr580 (Shp2Y580) were detected in the serially immunostained sections (Figures 6b and c). In six of the nine cases tested (Supplementary Table 1), we found increases in EphA2 expression as well as increases in the Shp2Y580 phosphorylation, suggesting that the increased expression of EphA2 in mammary cancer cells leads to the phosphorylation of Shp2.

We further investigated the phosphorylation of Erk in those cancer tissues to understand the Erk activation induced by EphA2 and Shp2 as we analyzed using cultured cells. The cancer tissues double positive for EphA2 and phospho-Shp2Y580 (six among nine tested in this study) were also phospho-Erk positive (Figure 6 and Supplementary Figure S4).

EphA2b is involved in the heart defects induced by Shp2T468M in zebrafish

The phenotypes of the patients with LEOPARD syndrome, such as cardiac defects, short trunk and increased distance between two eyes, can be reproduced in the zebrafish when zebrafish mutant Shp2 mRNAs corresponding to human LEOPARD syndrome mutant mRNAs are injected into the embryos.[21,22] By using the zebrafish model of LEOPARD syndrome, we first tested the significance of phosphorylation of Tyr542 and Tyr580 of Shp2 and second examined the involvement of EphA2 in the abnormal phenotype. The percentage of cardiac defects of the embryos injected with Shp2T468M/2YF mRNAs was less than those injected with Shp2T468M mRNAs, but more than those injected with wild-type Shp2 mRNAs and those uninjected (Figures 7a and b). These data indicate the importance of Tyr542 and Tyr580 for the cardiac abnormality and suggest the involvement Grb2-independent signaling, probably the Gab1-mediated signal as we found in the cultured cells (Figures 3h and i). Consistent with the results with cultured cells, the embryos injected with Shp2T468M mRNAs exhibited stronger Erk activation than those injected with wild-type Shp2 mRNAs, those injected with Shp2T468M/2YF mRNAs and those uninjected (Figure 7c).

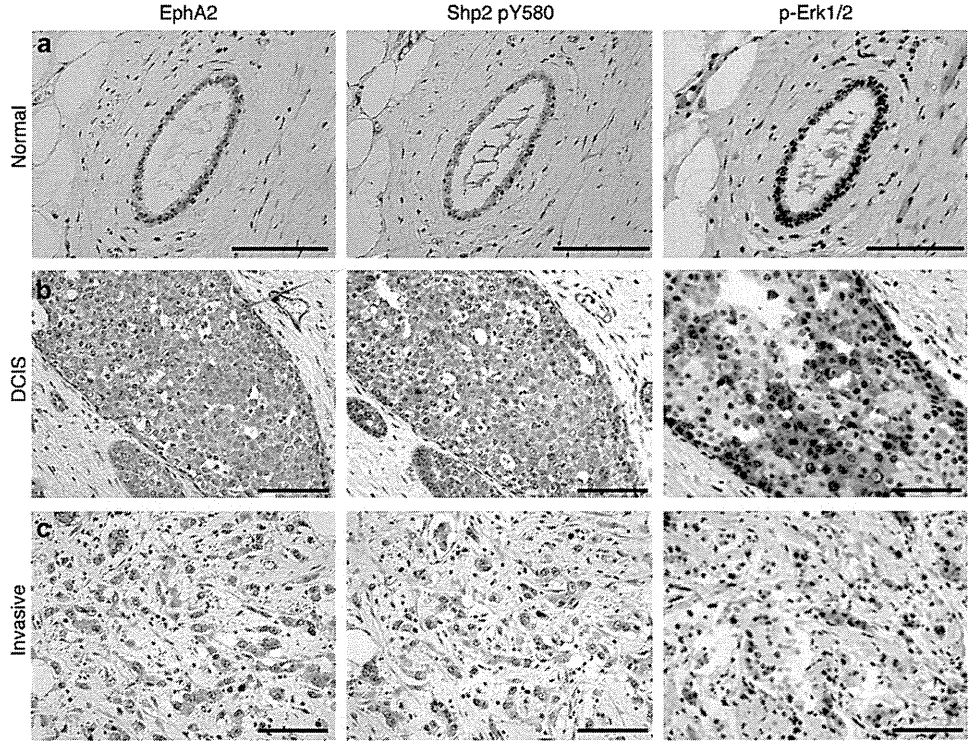

Figure 6. Phosphorylation of Shp2 and Erk1/2 in breast cancer expressing EphA2. Immunohistochemical analyses with the antibodies indicated on the top using specimens obtained from normal breast tissue (**a**), ductal carcinoma *in situ* (DCIS) (**b**) and invasive ductal carcinoma (**c**). Hematoxylin was used for counterstaining. Bar, 100 μm. Positive immunoreactivity is shown as brown color because of detection using 3,3′-diaminobenzidine (DAB) as described in the Materials and methods section.

To test the contribution of EphA2 to the defects found in zebrafish LEOPARD syndrome model, we knocked down the expression of EphA2. In zebrafish, two orthologs of human EphA2 (hereafter designated as EphA2a and EphA2b) are expressed.[23] Knockdown of EphA2a and EphA2b by morpholino oligos were confirmed by real-time reverse transcription–polymerase chain reaction (Figures 7d and e and Supplementary Figure S5). The heart defects found in the embryos injected with Shp2T468M mRNAs was suppressed by knockdown of EphA2b, but not by that of EphA2a (Figure 7f), suggesting the involvement of EphA2b in LEOPARD syndrome-like phenotypes in zebrafish. We then examined the expression of EphA2 in zebrafish hearts. *In situ* hybridization assay to detect EphA2 mRNAs revealed that neither EphA2a nor EphA2b mRNAs was expressed in the heart of normal embryos on the day 3 post-fertilization (Figure 7g). However, in the embryos injected with Shp2T468M mRNAs, both EphA2a and A2b mRNAs were detected in the heart (Figure 7h, Supplementary Figure S6 and Supplementary Table 2), suggesting that Shp2T468M promotes EphA2 expression.

We tested this possibility by examining whether Shp2T468M increases the expression of EphA2 in mammalian cultured cells. When Shp2T468M was overexpressed in NMuMG cells, the expression of EphA2 was increased (Figures 7i and j). Consistently, EphA2 mRNA was increased in NMuMG expressing Shp2T468M (Supplementary Figure S7a). This increase was significantly but not completely suppressed in the cells overexpressing Shp2T468M/2YF (Figures 7i and j). Similar to EphA2 expression, basal Erk activity and phosphorylation of Gab1 at Tyr627 was augmented by Shp2T468M and, to a lesser extent, by Shp2T468M/2YF (Figure 7i), suggesting the contribution of Shp2T468M-dependent Erk activation involving Gab1-mediated signal to the promotion of EphA2 expression. Because EphA2 is a direct transcriptional target of the Ras-Erk pathway,[24] we tested the effects of MEK inhibitor, U0126, on the induction of EphA2 protein by Shp2T468M. The increase in EphA2 and EphA2 mRNA by Shp2T468M was significantly suppressed by U0126 (Figures 7k and l and Supplementary Figure S7b). These results indicate that Shp2T468M enhances the expression of EphA2 via Erk-mediated signaling.

DISCUSSION

We identified EphA2 as a tyrosine kinase that phosphorylates Tyr542 and Tyr580 of Shp2 to enhance and prolong the Erk activation downstream of receptor tyrosine kinases in the cells stimulated with growth factors. Furthermore, we demonstrated the involvement of the Erk phosphorylation by EphA2-mediated phosphorylation of Shp2 in cancer progression and in an Shp2-associated disease, LEOPARD syndrome.

Shp2 is a positive regulator of Erk downstream of growth factor receptor signaling.[1–3] It remains controversial whether the phosphatase activity is required for Shp2-dependent Erk activation. Sprouty and the phosphorylation sites to which p120RasGAP binds are dephosphorylated by Shp2; therefore, Shp2 positively regulates Erk, because both tyrosine-phosphorylated Sprouty and p120RasGAP binding to phosphorylated tyrosines inactivate Ras-Erk signal pathway.[2,8,25,26] Shp2 functions not only as a phosphatase but also as a scaffold molecule to provide Grb2 binding sites by becoming phosphorylated at Tyr542/580 in its carboxy terminus. Therefore, the binding of Shp2 with Grb2 results in Erk activation in a manner independent of phosphatase activity of Shp2. It is important to clarify how Tyr542/580 are phosphorylated upon growth factor stimulation. In this study, we found that EphA2 directly phosphorylated these tyrosine residues (Figure 5d). The prolonged and enhanced Erk activation in the cells stimulated with growth factors were reduced in cells depleted of EphA2 (Figures 1c, e and g).

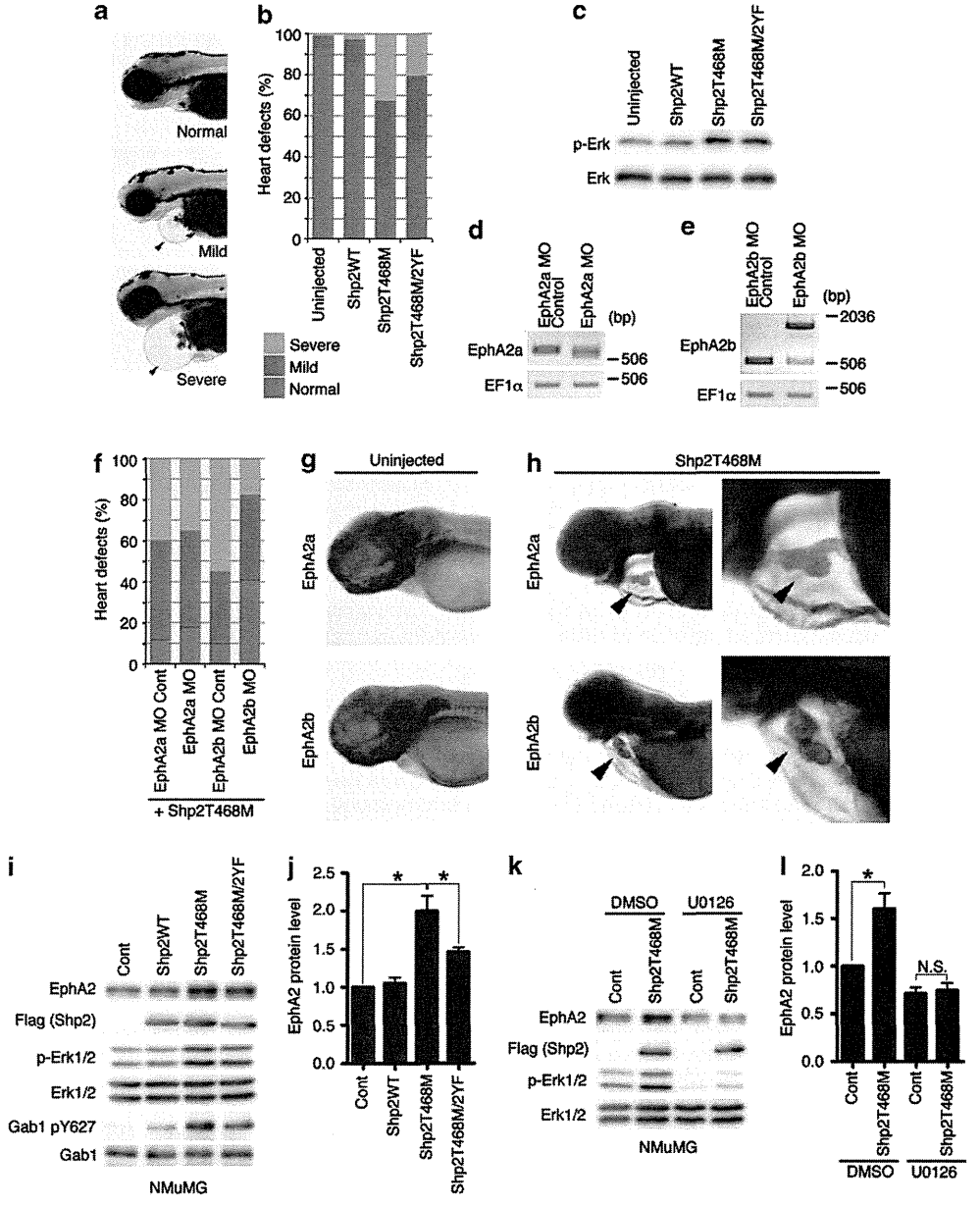

Figure 7. Shp2T468M associated with LEOPARD syndrome induces heart defects in zebrafish and promotes EphA2. (**a**) Heart defects in 3 days post-fertilization (dpf) zebrafish embryos after injection with Shp2T468M (200 pg per embryo) at one-cell stage embryos. Arrowheads indicate the cardiac edema. (**b**) Proportion of the phenotypes observed in the 3 dpf embryos injected with mRNAs ($n = 100–120$ per injection) indicated at the bottom was calculated according to the number of the normal or abnormal phenotypes of the fish among the total embryos subjected to the observation. The grade of abnormal cardiac edema was scored by the degree of the swelling. (**c**) Immunoblot analyses with the antibodies indicated at the left using the cell lysates prepared from the zebrafish embryos ($n = 10$) 8 h after injection with the mRNAs indicated on the top. (**d** and **e**) Reverse transcription–polymerase chain reaction (RT–PCR) analysis using primers for EphA2a, EphA2b or EF-1α and total RNA prepared from the zebrafish embryos 8 h after injection with morpholino oligos against EphA2a (4.2 ng per embryo) or EphA2b (8.4 ng per embryo) into one-cell stage embryos. (**f**) Proportion of the phenotypes of the 3 dpf embryos injected with Shp2T468M mRNA and the morpholino oligos as indicated on the bottom ($n = 100–120$ per injection) at one-cell stage embryos was analyzed as in (**b**). (**g**) Lateral views of 3 dpf embryos hybridized with probes indicated on the left. (**h**) Lateral views and their close-up images (right) of 3 dpf embryos injected with Shp2T468M mRNA at the one-cell stage and hybridized with probes indicated on the left. Arrowheads indicate the hearts. (**i**) Immunoblot analyses with the antibodies indicated at the left using the cell lysates prepared from NMuMG cells infected with the retrovirus vectors indicated on the top. (**j**) The result of quantitaive analyses of (**i**). The relative expression of EphA2 was calculated as the value of the expression of EphA2 induced by the infection with control virus was 1. The mean value with s.d. of four independent experiments was indicated. $^*P < 0.05$ among the four groups. (**k**) Immunoblot analyses with the antibodies indicated at the left using the cell lysates prepared from NMuMG cells infected with retrovirus vectors indicated on the top and treated with U0126 (20 μM) or dimethylsulfoxide (DMSO) for 24 h indicated on the top. (**l**) Expression of EphA2 observed in (**k**) was quantified as described in (**j**).

Simultaneous reduction of phosphorylation of Tyr542/580 was observed in those cells. Although ZAP70 is reported as a potential kinase that can phosphorylate Tyr542/580 in immune cells,[9] its expression in epithelial, endothelial and glial cells is unclear. Therefore, EphA2 seems to be responsible for the phosphorylation of Tyr542/580 in NMuMG epithelial cells, HUVECs and C6 glioma cells (Figures 1c, e and g). These results suggest that EphA2-dependent phosphorylation of Shp2 contributes to the

enhancement and prolongation of growth factor-induced Erk activation, although we cannot exclude the involvement of phosphatase activity of Shp2.

Mutations of *PTPN11* gene encoding Shp2 lead to the diseases that belong to the enhanced Ras-Erk signaling diseases.[4,5] When EphA2 was coexpressed, both phosphatase-active mutant Shp2 (Shp2N308D) and phosphatase-defective mutant Shp2 (Shp2T468M) induced more Erk activation than wild-type Shp2 (Figure 3b). These results suggest that Shp2 can induce Erk activation partly irrespective of its phosphatase activity. The binding of Shp2T468M to Grb2 requires the phosphorylation of Tyr542/580, concurring with the importance of phosphorylation of these residues for Shp2-mediated Erk activation.

Gab1 might function besides or together with Grb2 in mutant Shp2-induced Erk activation. Although wild-type Shp2 and mutant Shp2 (T468M and N308D) equally bound to Grb2, Erk was more phosphorylated in the cells expressing mutants than in those expressing wild-type Shp2 (Figure 3b). Binding of Gab1 to Shp2 is essential for HGF-dependent Erk activation.[16,27] Shp2T468M/2YF could induce weak phosphorylation of Erk when expressed with EphA2 than wild-type Shp2. Overexpression of a dominant-negative form of Grb2 could not completely inhibit the Erk activation in the cells expressing Shp2T468M and EphA2. These data suggest that phosphorylation of Tyr542/580 of Shp2 for Grb2 binding is not sufficient for full Erk activation by Shp2T468M.

In addition to the phosphatase activity, unfolding of Shp2 seems to be important to activate Erk as reviewed previously.[2] In the inactive Shp2 folding, the first SH2 domain of Shp2 is thought to bind to the phosphatase domain of Shp2 to block the association of the substrate with phosphatase domain. However, when Tyr542/580 are phosphorylated by unfolding, the former and the latter binds to the first SH2 and the second SH2 to allow the phosphatase domain to recognize the substrate by the active folding.[28,29] The cells expressing EphA2 with wild-type Shp2 did not show the activation of Erk, whereas those expressing EphA2 with either Shp2T468M or Shp2N308D showed the substantial Erk activation (Figure 3b). Thus, unfolding might be important for the activation mediated by EphA2. Activation of growth factor receptors induces the phosphorylation of adaptor scaffolding molecules for Shp2 binding to unfold Shp2. The significance of unfolding of Shp2 is also suggested in stomach cancer; CagA protein of *Helicobacter pylori* binds to Shp2 to activate Erk signaling by unfolding Shp2.[30] Therefore, without appropriate unfolding, overexpressed EphA2 and wild-type Shp2 might be incapable of activating Erk. These data suggest the dual roles of phosphorylated Tyr542 and Tyr580: for the active intramolecular folding to allow the exposure of phosphatase domain to its substrate and for the association of Shp2 with Grb2.

Our results indicate that Shp2T468M enhances Erk activation in zebrafish embryos at 8 hours postfertilization (hpf) (Figure 7c). However, it has been reported that another LEOPARD-associated mutant of Shp2, zShp2T462A, inhibits Erk activation in zebrafish embryos at 24 hpf.[22] It is still controversial whether the Erk is constitutively activated. In the induced pluripotent stem-derived cardiomyocytes, from the patient with LEOPARD syndrome, show an increase in activation of Erk.[6] The Erk activation might vary during development of the embryos expressing Shp2T468M. Further study is required to examine whether LEOPARD-associated mutants of Shp2 always function as a positive regulator for Erk activation.

The possible role of EphA2 in the phosphorylation of Shp2 was demonstrated in the breast cancers. The increase in EphA2 expression paralleled the phosphorylation of Tyr580 of Shp2 in the breast cancers (Figure 6). Therefore, Shp2 phosphorylated by increased EphA2 might recruit Grb2 to activate Ras-Erk signaling.[2,7,8] Consistently, phospho-Erk was detected in EphA2 and phospho-Shp2Y580 double-positive cancer specimens. The increased expression of EphA2 has been reported in other cancers.[11] In addition, EphA2 is suggested to activate Erk signaling without binding to ephrinA upon growth factor stimulation.[12,14] Thus, Shp2-dependent Erk activation signal involving Grb2 pathway may be hyperactivated in the malignant cancers that overexpress EphA2 to promote cancer cell proliferation. There are several points that should be explored: (1) How is EphA2 activated to phosphorylate Shp2 in the cells stimulated with growth factors? (2) Is the binding of ephrinA with EphA2 required for EphA2 activation? (3) How does Shp2T468M promote the expression of EphA2? However, at least the contribution of EphA2 to the Shp2-mediated Erk activation found in this study might account for the cell proliferation and invasion mediated by Erk in EphA2-expressing cancers.

In conclusion, EphA2 directly phosphorylates Tyr542/Tyr580 of Shp2 to recruit Grb2, thereby inducing Ras-Erk signal pathway in growth factor-induced signaling and cancers with the enhanced expression of EphA2. In the patients with LEOPARD syndrome, Gab1 might function to activate Erk besides or together with Grb2 (Supplementary Figure S8).

MATERIALS AND METHODS

EphA2 kinase assay

GST-Shp2 (amino acids (aa) 224–593) fusion protein was expressed and purified from *Escherichia coli* using glutathione sepharose. GST-EphA2 (aa 572–976) fusion protein was obtained from Carnabiosciences (Kobe, Japan). The recombinant GST-Shp2 (1 μg) and GST-EphA2 (40 ng) proteins were incubated in the kinase buffer (50 mM Tris-HCl (pH 7.4), 150 mM NaCl, 10 mM $MgCl_2$ and 1 mM ATP) for the time indicated. The reaction was stopped by adding EDTA to 20 mM. Phosphorylation of Shp2 was examined by immunoblotting using anti-Shp2 pY580 and anti-Shp2 pY542.

Immunohistochemistry

The studies involving human tissues from breast cancer patients were approved by the Medical Ethics Committee of Hokkaido University. In all cases, informed consent was obtained for the use of resected specimens. Paraffin-embedded sections were deparaffinized and rehydrated. Antigens were retrieved by boiling sections in citrate buffer (pH 6.0) for 10 min. Endogenous peroxidase was blocked with 3% H_2O_2. Sections were blocked with 5% normal goat serum and were incubated with rabbit polyclonal anti-EphA2 (1:500), anti-Shp2 pY580 (1:50) or anti-phospho-Erk1/2 (1:50) diluted with Can Get Signal immunostain solution A (Toyobo, Osaka, Japan) at room temperature for 1–2 h. After extensive washing in TBST, sections were detected with biotinylated goat anti-rabbit secondary antibody for 30 min followed by amplification with Vectastain ABC kit (Vector Laboratory, Burlingame, CA, USA), and were visualized with 3,3′-diaminobenzidine. Sections were counterstained with hematoxylin. Endothelial cells were used as positive internal controls for EphA2, phosphorylated Shp2 and phospho-Erk. Two board-certified pathologists independently assessed the immunostained slides. Any difference in the immunoreactivity of the cells was resolved by consensus. Immunoreactivity of the cells was assessed for staining intensity, which was scored on a scale of 0 to 3^+, with 0 being absence of staining, 1^+ being weakly, 2^+ being moderate and 3^+ being strongly immunoreactive.

Injection and *in situ* hybridization of zebrafish

Shp2 mRNAs were synthesized using mMESSAGEmMACHINE kit (Ambion, Austin, TX, USA). Morpholino oligos and synthetic mRNAs were injected into the blastomere of one-cell stage embryos. Whole-mount *in situ* hybridization was performed according to the conventional method. The experiments using zebrafish was approved by the animal committee of National Cerebral and Cardiovascular Center and was performed according to the guideline for the animal use provided by the committee.

Statistical analysis

We analyzed the difference in values among multiple groups by one-way analysis of variance followed by Bonferroni's post-test and that of the two groups by two-tailed *t*-test using Prism (GraphPad Software, San Diego, CA, USA). The values are expressed as means with s.d. P-values < 0.05 were considered statistically significant.

CONFLICT OF INTEREST

The authors declare no conflict of interest.

ACKNOWLEDGEMENTS

We thank M Matsuda (Kyoto University), T Akagi (KAN Research Institute), T Hirano (Osaka University) and S Kunimoto (Nippon University) for reagents; M Masuda, S Fukuhara and H Fukui for valuable advice; and M Sone, K Hiratomi, M Minamimoto, H Yonekawa, W Koeda and Y Matsuura for technical assistance. This work was supported, in part, by grants from the Ministry of Education, Science, Sports and Culture of Japan; the Ministry of Health, Labor and Welfare of Japan; Takeda Science Foundation; and AstraZeneca Research Grant.

REFERENCES

1 Chan G, Kalaitzidis D, Neel BG. The tyrosine phosphatase Shp2 (PTPN11) in cancer. *Cancer Metastasis Rev* 2008; **27**: 179–192.
2 Dance M, Montagner A, Salles JP, Yart A, Raynal P. The molecular functions of Shp2 in the Ras/mitogen-activated protein kinase (ERK1/2) pathway. *Cell Signal* 2008; **20**: 453–459.
3 Grossmann KS, Rosario M, Birchmeier C, Birchmeier W. The tyrosine phosphatase Shp2 in development and cancer. *Adv Cancer Res* 2010; **106**: 53–89.
4 Tidyman WE, Rauen KA. The RASopathies: developmental syndromes of Ras/MAPK pathway dysregulation. *Curr Opin Genet Dev* 2009; **19**: 230–236.
5 Tartaglia M, Gelb BD. Disorders of dysregulated signal traffic through the RAS-MAPK pathway: phenotypic spectrum and molecular mechanisms. *Ann NY Acad Sci* 2010; **1214**: 99–121.
6 Carvajal-Vergara X, Sevilla A, D'Souza SL, Ang YS, Schaniel C, Lee DF *et al.* Patient-specific induced pluripotent stem-cell-derived models of LEOPARD syndrome. *Nature* 2010; **465**: 808–812.
7 Araki T, Nawa H, Neel BG. Tyrosyl phosphorylation of Shp2 is required for normal ERK activation in response to some, but not all, growth factors. *J Biol Chem* 2003; **278**: 41677–41684.
8 Cleghon V, Feldmann P, Ghiglione C, Copeland TD, Perrimon N, Hughes DA *et al.* Opposing actions of CSW and RasGAP modulate the strength of torso RTK signaling in the *Drosophila* terminal pathway. *Mol Cell* 1998; **2**: 719–727.
9 Cha Y, Park KS. SHP2 is a downstream target of ZAP70 to regulate JAK1/STAT3 and ERK signaling pathways in mouse embryonic stem cells. *FEBS Lett* 2010; **584**: 4241–4246.
10 Lemmon MA, Schlessinger J. Cell signaling by receptor tyrosine kinases. *Cell* 2010; **141**: 1117–1134.
11 Ireton RC, Chen J. EphA2 receptor tyrosine kinase as a promising target for cancer therapeutics. *Curr Cancer Drug Targets* 2005; **5**: 149–157.
12 Brantley-Sieders DM, Zhuang G, Hicks D, Fang WB, Hwang Y, Cates JM *et al.* The receptor tyrosine kinase EphA2 promotes mammary adenocarcinoma tumorigenesis and metastatic progression in mice by amplifying ErbB2 signaling. *J Clin Invest* 2008; **118**: 64–78.
13 Pasquale EB. Eph-ephrin bidirectional signaling in physiology and disease. *Cell* 2008; **133**: 38–52.
14 Pasquale EB. Eph receptors and ephrins in cancer: bidirectional signalling and beyond. *Nat Rev Cancer* 2010; **10**: 165–180.
15 Edouard T, Montagner A, Dance M, Conte F, Yart A, Parfait B *et al.* How do Shp2 mutations that oppositely influence its biochemical activity result in syndromes with overlapping symptoms? *Cell Mol Life Sci* 2007; **64**: 1585–1590.
16 Cunnick JM, Dorsey JF, Munoz-Antonia T, Mei L, Wu J. Requirement of SHP2 binding to Grb2-associated binder-1 for mitogen-activated protein kinase activation in response to lysophosphatidic acid and epidermal growth factor. *J Biol Chem* 2000; **275**: 13842–13848.
17 Wang Y, Ota S, Kataoka H, Kanamori M, Li Z, Band H *et al.* Negative regulation of EphA2 receptor by Cbl. *Biochem Biophys Res Commun* 2002; **296**: 214–220.
18 Miao H, Li DQ, Mukherjee A, Guo H, Petty A, Cutter J *et al.* EphA2 mediates ligand-dependent inhibition and ligand-independent promotion of cell migration and invasion via a reciprocal regulatory loop with Akt. *Cancer Cell* 2009; **16**: 9–20.
19 Fang WB, Brantley-Sieders DM, Hwang Y, Ham AJ, Chen J. Identification and functional analysis of phosphorylated tyrosine residues within EphA2 receptor tyrosine kinase. *J Biol Chem* 2008; **283**: 16017–16026.
20 Araujo J, Logothetis C. Dasatinib: a potent SRC inhibitor in clinical development for the treatment of solid tumors. *Cancer Treat Rev* 2010; **36**: 492–500.
21 Jopling C, van Geemen D, den Hertog J. Shp2 knockdown and Noonan/LEOPARD mutant Shp2-induced gastrulation defects. *PLoS Genet* 2007; **3**: e225.
22 Stewart RA, Sanda T, Widlund HR, Zhu S, Swanson KD, Hurley AD *et al.* Phosphatase-dependent and -independent functions of Shp2 in neural crest cells underlie LEOPARD syndrome pathogenesis. *Dev Cell* 2010; **18**: 750–762.
23 Lemeer S, Ruijtenbeek R, Pinkse MW, Jopling C, Heck AJ, den Hertog J *et al.* Endogenous phosphotyrosine signaling in zebrafish embryos. *Mol Cell Proteomics* 2007; **6**: 2088–2099.
24 Macrae M, Neve RM, Rodriguez-Viciana P, Haqq C, Yeh J, Chen C *et al.* A conditional feedback loop regulates Ras activity through EphA2. *Cancer Cell* 2005; **8**: 111–118.
25 Hanafusa H, Torii S, Yasunaga T, Nishida E. Sprouty1 and Sprouty2 provide a control mechanism for the Ras/MAPK signalling pathway. *Nat Cell Biol* 2002; **4**: 850–858.
26 Agazie YM, Hayman MJ. Molecular mechanism for a role of SHP2 in epidermal growth factor receptor signaling. *Mol Cell Biol* 2003; **23**: 7875–7886.
27 Cai T, Nishida K, Hirano T, Khavari PA. Gab1 and SHP-2 promote Ras/MAPK regulation of epidermal growth and differentiation. *J Cell Biol* 2002; **159**: 103–112.
28 Lu W, Gong D, Bar-Sagi D, Cole PA. Site-specific incorporation of a phosphotyrosine mimetic reveals a role for tyrosine phosphorylation of SHP-2 in cell signaling. *Mol Cell* 2001; **8**: 759–769.
29 Neel BG, Gu H, Pao L. The 'Shp'ing news: SH2 domain-containing tyrosine phosphatases in cell signaling. *Trends Biochem Sci* 2003; **28**: 284–293.
30 Higashi H, Tsutsumi R, Muto S, Sugiyama T, Azuma T, Asaka M *et al.* SHP-2 tyrosine phosphatase as an intracellular target of Helicobacter pylori CagA protein. *Science* 2002; **295**: 683–686.

Supplementary Information accompanies this paper on the Oncogene website (http://www.nature.com/onc)